View metadata, citation and similar papers at core.ac.uk

brought to you by CORE

provided by Ghent University Academic Bibliography

Selecting conversion phosphors for white light-emitting diodes

Philippe F. Smet, Anthony B. Parmentier and Dirk Poelman

LumiLab, Department of Solid State Sciences, Ghent University, Ghent, Belgium

Corresponding author: philippe.smet@ugent.be, +32 9 264 43 53

This is the peer-reviewed version of the paper published in:

Journal of the Electrochemical Society, **158** (2011) R37-R54

An updated version can be found at:

http://dx.doi.org/10.1149/1.3568524

Abstract

Light emitting diodes (LEDs) are on the verge of a breakthrough in general lighting, due to their rapidly improving efficiency. Currently, white LEDs with high color rendering are mainly based on wavelength conversion by one or more phosphor materials. This Review first describes how to quantify the quality of a light source, discussing the color rendering index (CRI) and alternative color quality indices. Then, six main criteria are identified and discussed, which should be fulfilled by a phosphor candidate to be considered for actual application in LEDs. These criteria deal with the shape and position of the emission and the excitation spectra, the thermal quenching behavior, the quantum efficiency, the chemical and thermal stability and finally with the occurrence of saturation effects. Based on these criteria, the most common dopant ions (broad-band emitting Eu^{2+}, Ce^{3+} and Mn^{2+}, line-emitting rare earth ions,...) and host compounds (garnets, sulfides, (oxy)nitrides,...) are

Selecting conversion phosphors for white light-emitting diodes

Philippe F. Smet, Anthony B. Parmentier and Dirk Poelman

LumiLab, Department of Solid State Sciences, Ghent University, Ghent, Belgium

Corresponding author: philippe.smet@ugent.be, +32 9 264 43 53

Abstract

Light emitting diodes (LEDs) are on the verge of a breakthrough in general lighting, due to their rapidly improving efficiency. Currently, white LEDs with high color rendering are mainly based on wavelength conversion by one or more phosphor materials. This Review first describes how to quantify the quality of a light source, discussing the color rendering index (CRI) and alternative color quality indices. Then, six main criteria are identified and discussed, which should be fulfilled by a phosphor candidate to be considered for actual application in LEDs. These criteria deal with the shape and position of the emission and the excitation spectra, the thermal quenching behavior, the quantum efficiency, the chemical and thermal stability and finally with the occurrence of saturation effects. Based on these criteria, the most common dopant ions (broad-band emitting Eu^{2+}, Ce^{3+} and Mn^{2+}, line-emitting rare earth ions,...) and host compounds (garnets, sulfides, (oxy)nitrides,...) are evaluated. Although many phosphor materials have been proposed in literature in recent years, the number of phosphors effectively fulfilling all six requirements is relatively small.

1. Introduction.

The history of light emitting diodes (LEDs) goes back more than a century. Already in 1907, H. J. Round published on light emission from a silicon carbide junction diode, the first light emitting diode (LED) ever. Independently, Losev observed emission from ZnO and SiC diodes, as published in 1927 [1]. At that time, the potential of the technology was not realized and the inventions remained largely unnoticed. It was not until 1962 that the first practical visible spectrum LED was developed, by Nick Holonyak at General Electric. In the decades that followed, LEDs were used extensively in numerical displays and signaling applications. However, only around 1995 high brightness and blue LEDs were developed, which made it possible to use LEDs for general lighting.

Nowadays, LEDs use a mature technology which can compete with the traditional incandescent and (compact) fluorescent lamps (Fig. 1) [2]. They have numerous advantages over the latter, such as small size, high lifetime, robustness, fast switching and an efficiency which starts to approach the theoretical limits. It is well recognized that the widespread replacement of (incandescent) lamps by higher efficiency light sources will lead to a considerable reduction of the worldwide electricity consumption, corresponding to the energy produced by about 140 power plants of average size in the US alone, for a 40% market penetration and an luminous efficacy of 150lum/W [3]. The current attention to energy saving and reduction of CO_2 emission in the atmosphere should therefore give an additional boost to the development of LEDs for lighting. Remaining disadvantages of LEDs are the need for extensive cooling of high power devices (ultimately limiting the maximum power per LED chip), the need for current driving and the lack of high color quality white LEDs. Such white LEDs are typically made starting from a blue emitting LED and converting part of its light to green and red by means of one or more phosphor materials. There are only a limited number of phosphor materials

known that are suitable for this wavelength conversion. The present review is focused on six main performance requirements for state-of-the-art color conversion phosphors:

1. An emission spectrum that, in combination with the emission of the other components (LED, other phosphors), leads to a pure white emission with a specific color rendering and color temperature.
2. An excitation spectrum showing good overlap with the pumping LED and large absorption strength.
3. An emission spectrum, excitation spectrum and a quantum efficiency that remain unchanged at elevated temperature.
4. A quantum efficiency approaching unity, thus maximizing the overall electrical-to-optical conversion efficiency of the entire LED-phosphor package.
5. An excellent chemical and temperature stability.
6. Absence of emission saturation at high fluxes.

This review paper is structured as follows. First (Section 2) important parameters related to the determination of the color quality (i.e. how naturally are colors reproduced under illumination with an artificial light source) and the efficiency of a light source, as perceived by the human eye, are discussed. In Section 3, two different approaches to obtain white light sources using LEDs are discussed: the RGB-method using three LEDs and the phosphor-converted LED (pcLED). For the latter, differentiation is made for blue and UV pumping LEDs. Section 4 elaborates the six abovementioned requirements for LED conversion phosphors. Finally, several classes of phosphor materials are evaluated against these requirements and future directives are given. In conclusion, we will show that the future for LEDs is bright, but that the number of currently available high-performance conversion phosphors is still limited, in spite of the large number of ‘new’ host-dopant combinations that have been recently reported. Research into photoluminescent materials should therefore continue, albeit with a more focused approach, to which this Review hopes to contribute.

2. What is the ideal light source and how to quantify it?

When looking for the 'ideal' emission spectrum of LEDs we will limit ourselves to general lighting applications, both indoors and outdoors. Of course, it is theoretically possible to use any visible spectrum, or even monochromatic light, for lighting. However, we will specifically aim for white light only, as this is the type of light with the most universal applications. In addition, it is the type of light source that can be used as a replacement of incandescent, quartz halogen or CFL (compact fluorescent) lamps.

In order to determine whether the spectrum of a light source is suitable for general lighting, three main evaluation criteria can be considered: the efficiency of the radiation (not radiometric but as perceived by the human observer), the color quality of the light and the absence of harmful radiation. Finally, in section 2.4, the color quality of a light source is revisited, and the 'traditional' CRI (color rendering index) approach is compared to recent approaches, such as the CQS (color quality scale).

2.1. The luminous efficiency of the radiation.

The LER or luminous efficiency of the radiation, in lumen per watt, is a parameter describing how bright the radiation is perceived by the average human eye. It scales with the eye sensitivity curve *V(λ)* (Fig. 2) and can be calculated from the emission spectrum *I(λ)* as:

$$\mathrm{LER}(lm/W) = 683 lm/W \cdot \frac{\int_{360nm}^{830nm} I(\lambda)V(\lambda)d\lambda}{\int_{360nm}^{830nm} I(\lambda)d\lambda} \quad (1)$$

As the eye sensitivity peaks at 555 nm, the highest possible LER (683 lm/W) is obtained from monochromatic – green – radiation at 555 nm. Therefore, 683 lm/W is the highest possible efficiency that can ever be obtained from a light source: When 100% of the electrical power is converted to

light at a wavelength of 555 nm, the efficiency of the light source is 683 lm/W. Any other spectrum will yield a lower LER, as the human eye is less sensitive for other wavelengths. For obtaining white light, emission in the red and blue is necessary (which we will discuss in detail later), so the LER of white light is significantly lower than 683 lm/W, being in the order of 350 lm/W. In general, one has to find a compromise between high LER and good color quality of the light source, as discussed in [4]. Alternative abbreviations for LER have been used, such as the PSLE (photopic spectral luminous efficacy) [5].

At very low light levels, typically below 1 cd/m^2, the rods of the retina, responsible for night vision, start to play a role. The peak sensitivity of the rods lies at lower wavelength, at 504 nm (Fig. 2), and they are much more sensitive than cones. Thus the human eye sensitivity gradually shifts from photopic vision at high light intensities to scotopic vision in the low light level regime. In the intermediate range, called the mesopic regime, the intensity and wavelength sensitivity changes in a complex way, making it difficult to describe eye response in an accurate way [6], [7]. As in the majority of lighting applications, the observed light intensity is well into the photopic range, we will not bother with the complexities of mesopic and scotopic vision in the present discussion.

2.2. The color 'quality' of the light source.

Since the work of the CIE in the early 20th century, culminating in the publication of the CIE standard observer in 1931, it is well known how to obtain a specific color (specified by its color coordinates (x,y)) from a set of primary sources. This is the basis of modern *display* technology: suitable blue, green and red (RGB) primary colors can be combined to form any color within the triangle, formed by the color coordinates of the 3 primaries. White emission is then obtained by combining all 3 primaries in suitable amounts. Basically, a set of 3 primary sources with the correct color coordinates

(specified in standards by institutions like the EBU, the European Broadcasting Union and SMPTE, the Society for Motion Picture and Television Engineers) is all that is needed to make a color display: the specific emission spectrum of the primaries is not important, only its color coordinates. Therefore, good color rendering of emissive displays is a relatively easy job.

Making a good light source for general illumination is much more difficult. The human eye responds in such a way to optical stimuli that there is no 'one to one' correspondence between a spectrum and the observed color. Indeed, two lamps can look, for example, equally white but have a completely different emission spectrum. Although the lamps may look the same when viewed directly, they are not equivalent (even if they possibly have the same LER). We will discuss the color quality of light sources in detail in section 2.4.

2.3. Radiation safety.

We will not be concerned with electrical safety or problems of hazardous waste, although the latter has been the subject of recent debate, as CFLs (compact fluorescent lamps) typically contain minute amounts of mercury [8]. The question here is whether the lamp emission spectrum is safe and healthy to human, animal and plant life. The first and main concern is whether there is any ultraviolet emission from the lamp which could be harmful. Lamps for sun beds obviously pose a potential risk [9], but white fluorescent lamps have also been investigated for their UV safety. However, based on the guidelines for exposure limits to ultraviolet radiation [10], it was concluded that skin exposure to fluorescent lighting does not pose any problem except for very photosensitive people, as the average UV dose from fluorescent lamps is only of the order of 5% of the dose received from daylight exposure [11]. In a recent study of a large number of commercially available CFLs by Khazova et al. [12], it was concluded that CFLs with single glass envelopes do pose a certain potential risk of skin overexposure at close proximity to the lamp. In view of the present review, we should have a look at

the potential risks involved in the use of phosphor converted UV LEDs. Assuming an LED with an emission wavelength of 395 nm, the integrated maximum exposure limit for an 8 hour exposure per day is about 80 J/cm^2 or 3 mW/cm^2 [10]. As much higher power densities than 3 mW/cm^2 are available from modern 395 nm LEDs, it is clear that the 395 nm radiation should be well absorbed by the wavelength conversion materials, or that a minimum distance from the source should be observed. As the human eye sensitivity is extremely low at 395 nm, the direct radiation hardly contributes to the perceived brightness of the light source anyway.

Also for white LEDs, eye safety should be considered. Although the power of LEDs is currently limited to only a few watt per chip, leading to a limited irradiance (in W/m^2) or, in photometric units, illuminance (in lux), LEDs are close to point sources. Consequently, the corresponding radiance (in Wm^{-2}sr^{-1}) or luminance (in cdm^{-2}) can be quite large.

The maximum allowed long-term exposure of the human eye is specified as 100 Wm^{-2}sr^{-1}, at a wavelength of 440 nm [13]. This limit relaxes to higher values for lower and longer wavelengths (therefore the name 'blue-light hazard'). Even while typical high power white and blue LEDs only reach radiances of the order of 10 Wm^{-2}sr^{-1}, their emission is considered having a 'moderate risk' [14]. Indeed, for point sources with an apparent size of less than 11 mrad (a 1 mm spot seen from a distance of 9 cm), the exposure limit for 'low risk' is specified in irradiance units as 100/t Wm^{-2}, with t the exposure time in seconds, and 0.01 Wm^{-2}sr^{-1} for times longer than 10000 s. Modern LEDs reach values well in the 10 Wm^{-2} range and thus are considered unsafe. Nevertheless it can be assumed that the observer will not be staring at the light source for a long time due to normal eye movements, and therefore the radiation will be spread over the retina with time. Due to the natural aversion response, long exposures are unrealistic and the actual risk is low. As bare LED chips as light sources are obviously unsafe when deliberately stared at, it is imperative that fixture designers take care of sufficiently shielding the direct view of the LED.

Next to these direct radiation hazards, a number of clinical investigations have been performed on the physiological effects of certain types of visible radiation. For example, it was found that exposure to short-wavelength light at around 460 nm is effective in suppressing melatonin secretion [15]. As melatonin, being produced during the sleeping phase, plays an important role in controlling the circadian system [16], lighting designers should choose specific spectral distributions depending on the application: short wavelengths are bound to keep people awake, while low CCT (warm white) light of 2300 K does not suppress melatonin production [15] and would be ideal for evening indoor lighting. Other studies have investigated the effects of lighting on seasonal depression, physical activity levels [11], cognitive performance [17] and even the cutaneous temperature of the feet [18].

2.4. Color rendering (CRI and CQS)

An ideal light source for general lighting should thus combine a maximum LER with perfect color rendering. While the LER can be unambiguously calculated, the definition of 'good' color rendering is a matter of ongoing debate. The currently used standard for color rendering, introduced by the CIE in 1965 [19], updated in 1974 [20] and republished with minor corrections in 1995 [21], is the CRI or color rendering index. For the rest of the discussion, it is valuable to summarize the definition of this CRI. A full description of the standard can be found in the excellent book by Schanda [22]. The CRI definition is based on comparing the color of test objects when illuminated by the light source under test, to the colors of the objects illuminated by a reference source. Obviously, the choice of this reference is very important, since it defines what the 'true' colors of objects are. In the definition of the CRI, an infinite number of reference sources is used, depending on the type of test source: first, the spectrum of the test source is compared to that of a black body radiator, and the temperature of the black body that most closely matches the spectrum of the test source is called the correlated

color temperature (CCT) of the test source. When the CCT of the test source is below 5000 K, the reference source used for the calculation of the CRI is a black body radiator of the same CCT. Above 5000 K, a standard daylight spectrum of the same CCT, derived from the D65 standard illuminant and defined by the CIE [23] is used. Fourteen different color test samples are used, of which the first eight are used for calculating the general color rendering index R_a. The colors of the test objects are specified in the CIE 1964 uniform color space, the CIE U*V*W* space [22]. Dependent on the test source, a chromatic adaptation correction is applied, as observers tend to identify colors objects in the same way, even if the CCT of the light source is highly different. The general color rendering index R_a is then calculated as:

$$R_a = 100 - 4.6 \cdot \frac{1}{8} \sum_{i=1,\ldots,8} \Delta E_i \qquad (2)$$

With ΔE_i the distance between the colors of test object *i* illuminated with test and reference source, calculated in the U*V*W* uniform color space.

The merit of the CRI as defined above, is that it allows to describe the color rendering ability of any light source with a single number. However, it was realized that the definition of the CRI is far from perfect [24], and several improvements were proposed, leading to a new standard in 1996, the general color rendering index R_{96a}; however, this standard has not been adopted in practice. The most complete set of improvements on the CIE standard was recently proposed by Davis and Ohno [25], leading to a new index, the CQS or color quality scale. The main differences with the CRI are [26]:

- A different color space is used. When calculating differences in color based on the geometrical distance between color coordinates, it is important that the color space used is as uniform as possible. In the CQS, the CIE 1976 (CIELAB) color space [22] is used, which is more uniform than the U*V*W* color space, used in calculating the CRI, which is now considered obsolete.

- The calculation is performed on a larger set of 15 different color samples, which are more saturated in color than the 8 original CIE samples.
- R_a is calculated from the mean difference in color of the 8 test samples. This implies that a large difference in color for only one sample only gives a small penalty to the color rendering index. In the CQS calculation, the root mean square deviation in color is used, which penalizes large differences more severely.
- Since the adoption of the CRI, more advanced models for chromatic adaptation have been developed. The CQS – which is still under development – will include an update from the Von Kries chromatic adaptation correction, which is considered outdated [25].

  A minor, but somewhat awkward drawback of the CRI is that there is no minimum value zero for the general color rendering index R_a. For example, calculation yields R_a = -47 for low pressure sodium lamps. The CQS uses a normalization equation to overcome this problem and yield a range of values between 0 and 100:

$$R_{\text{new}} = 10 \ \ln\left[\exp(R_{\text{old}}/10) + 1\right] \tag{3}$$

- Very often, observers prefer to see objects in more vivid and saturated colors over types of illumination that yield a dull appearance. This has led to the development of a number of indices describing how 'nice' objects look under the test illuminant. Early work includes the 'flattery index' by Judd [27] and the 'preference index' by Thornton [28]. These studies conclude that objects can look better under certain test light sources than under natural light, which would, in terms of a CRI, yield an index higher than 100. Obviously, any color differences between illumination with a test source and the reference yield a R_a lower than 100, as the reference source is considered as the 'perfect' source. In the definition of the CQS, light sources that yield color rendering of objects with the same hue but higher saturation than the reference source, are not penalized but are given the same 'ideal' CQS-index.

- In the CRI, even light sources with a very high (bluish) and very low (reddish) CCT can yield a high value for R_a, as also the reference source used has this very high or low CCT. However, the subjective color rendering ability of such light sources is low: indeed, they only allow the reproduction of a smaller color gamut, and colors are perceived as unnatural. The CQS therefore assigns a lower rendering index for these light sources, roughly scaling with the area of the color gamut of the 15 color samples.

It is clear that the CQS includes a large number of incremental improvements over the definition of the CRI, without being revolutionary. One of the main limitations is that it still depends on the choice of a reference light source, or, in this case, an infinite number of reference sources, as the reference depends on the CCT of the test source.

Next to the efforts by Judd and Thornton mentioned before, a large number of research groups have tried to find metrics which describe the color rendering properties of light sources more accurately, and a number of them were reviewed in [29]. Essentially, color quality indices can be divided in two classes. One class compares the rendered colors to those of a reference light source (like the CRI and the CQS). Others, like the flattery index [27], preference index [28], FCI (feeling of contrast index) [30] and HRI (color harmony index) [31] try to quantify the naturalness, vividness, color gamut area or harmony between colors. In the latter case, the aim is not to reproduce colors correctly (as far as the colors are correct when objects are illuminated with the reference source), but to find a light source which yields colors that look 'right' or 'nice'. We agree with several other authors that it is probably impossible to find a single index which describes the color quality of light sources sufficiently accurately, and that several indices will have to supplement each other [29-31].

In 2006, a CIE technical committee (TC1-69) was established to "investigate new methods for assessing the colour rendition properties of white-light sources used for illumination, including solid-state light sources, with the goal of recommending new assessment procedures".

The inherent difficulty to define what a good light source is can be summarized by the Latin proverb "De gustibus et coloribus non est disputandum": "There's no arguing about tastes and colors". Incidentally, it is directly applicable to our present problem.

3. White light approaches using LEDs.

Given that light emitting diodes produce quasi-monochromatic light (i.e. with a narrow emission band), basically two approaches can be followed to obtain a white LED. On the one hand, a combination of (at least) three LEDs, with power ratios adjusted to obtain white light with a specific color temperature. On the other hand, a single LED can be used in combination with one or more phosphor materials to partially or fully convert the LED emission (Fig. 3).

3.1. RGB-LEDs.

The approach of using only LEDs (without phosphor convertors) has some specific advantages. First of all, conversion losses associated with the use of phosphors are eliminated. Furthermore, it also allows the development of smart light sources, which can adapt their emission color (from the primary colors to white light with variable color temperature) and intensity upon specific circumstances or as desired by the user. Besides general lighting applications, which require only a fixed color and intensity, there certainly exists a large market for this type of smart light sources.

The relatively narrow emission bands of LEDs and the possibility to choose the peak emission wavelengths, allow producing light sources characterized by a high LER in combination with a

reasonable color rendering. However for an improved color rendering, a combination of four LEDs seems necessary. This is quantified in section 4.1.

A disadvantage is that more complex electronics (possibly with feedback mechanisms [32]) have to be used to counteract the differential ageing of the current red, green and blue LEDs. Both current and temperature dependent color shifts are problematic when dimming an RGB-LED combination while maintaining the emission color. The spectral shifts are in general not equal for these LEDs as function of the driving current and the chip temperature (which is of course related to the driving current, but also dependent on the ambient temperature and the cooling of the entire device) [33]. As smart LED-based light source rely on both a choice of intensity and color, considerable development effort has to be put in the design of phosphor-free light sources.

3.2. Phosphor converted LEDs.

In contrast to the RGB approach, a single LED light source can be combined with one or more conversion phosphors to obtain white light (Table 1). Currently, most of the commercially available LED-based white light sources rely on this approach. Until recently, these were almost solely based on the combination of a blue LED and an YAG:Ce^{3+}-based phosphor. Basically, two approaches can be discerned. One can use a blue LED and convert part of the emitted light to longer wavelengths by use of a phosphor material, or one can fully convert the emission from a (near)ultraviolet LED by phosphors.

Table 1. Key parameters for selected phosphor-converted white LEDs (phosphor composition, color temperature and color rendering). Estimated values are denoted by *.

$\lambda_{max,LED}$ (nm)	Phosphor(s)	CCT (K)	CRI	Ref
460	$Y_3Al_5O_{12}:Ce^{3+}$	5600	71	[34]
460*	$Y_3Al_5O_{12}:Ce^{3+}$, $CaS:Eu^{2+}$	5500	92	[35]
460	$Y_3Al_5O_{12}:Ce^{3+}$, $Sr_2Si_5N_8:Eu^{2+}$	2900	80	[36]
460	$Sr_2GaS_4:Eu^{2+}$, $SrS:Eu^{2+}$	3600	82	[37]
460	$Sr_2GaS_4:Eu^{2+}$, $(Ca,Sr)S:Eu^{2+}$	4800	92	[38]
450	$Ca_3Sc_2Si_3O_{12}:Ce^{3+}$, $CaAlSiN_3:Eu^{2+}$	6500*	92	[39]
450	$SrSi_2O_2N_2:Eu^{2+}$, $Sr_2Si_5N_8:Eu^{2+}$	3200	89	[40]
455	$SrSi_2O_2N_2:Eu^{2+}$, $CaSiN_2:Ce^{3+}$	5200	91	[41]
450	$(Sr,Ca)_3(Al,Si)O_4(O,F):Ce^{3+}$, $K_2TiF_6:Mn^{4+}$	3200	90	[42]
455	$BaSi_2O_2N_2:Eu^{2+}$, β-SiAlON:Eu^{2+}, Ca-α-SiAlON:Eu^{2+}, $CaAlSiN_3:Eu^{2+}$	6400	96	[43]
455	$BaSi_2O_2N_2:Eu^{2+}$, β-SiAlON:Eu^{2+}, Ca-α-SiAlON:Eu^{2+}, $CaAlSiN_3:Eu^{2+}$	2900	98	[43]
365	$BaMgAl_{10}O_{17}:Eu^{2+}$, $Ca_9La(PO_4)_7:Eu^{2+}$,Mn^{2+}	4500	92	[44]

Before discussing advantages and disadvantages of both approaches, we look at the conversion efficiency, as obviously larger energy losses are inevitable when the exciting photon from the LED and the emitted photon from the phosphor have a large difference in wavelength. In general the conversion efficiency $\eta_{e\text{-}o}$ of electrical power to optical power (irrespective of the sensitivity of the human eye) for the entire LED package (chip (*L*) and phosphor(*P*)) can be written as

$$\eta_{e-o} = \frac{P_{opt}}{P_{el}} = \eta_L \sum_i f_i Q_{P,i} \frac{\overline{\lambda}_L}{\overline{\lambda}_{P,i}} \tag{4}$$

$$\text{with} \qquad \eta_L = \frac{P_{opt,L}}{P_{el,L}}, \quad \sum_i f_i = 1 \quad \text{and} \quad \overline{\lambda} = \frac{\int I(\lambda)\lambda d\lambda}{\int I(\lambda) d\lambda} \tag{5}$$

with η_L the electrical to optical power conversion efficiency of the LED chip alone. f_i is the fraction of the light intensity emitted by the LED which is absorbed by phosphor *i*, $Q_{P,i}$ is the internal quantum efficiency of the phosphor (see section 4.4) and $\overline{\lambda}$ is the barycenter of the emission spectrum of the LED or phosphor. This conversion efficiency $\eta_{e\text{-}o}$ is also called the wall-plug efficiency (WPE) [37]. In the case of a blue LED in combination with a single phosphor (*B*) and an UV LED in combination with two phosphors (*UV*), these equations can be rewritten as

$$\eta_{\mathrm{e-o,B}} = \eta_{\mathrm{L,B}} \left[f + (1-f) Q_{\mathrm{P}} \frac{\overline{\lambda}_{\mathrm{L,B}}}{\overline{\lambda}_{\mathrm{P}}} \right] \tag{6}$$

$$\eta_{\mathrm{e-o,UV}} = \eta_{\mathrm{L,UV}} \left[f Q_{\mathrm{P}_1} \frac{\overline{\lambda}_{\mathrm{L,UV}}}{\overline{\lambda}_{\mathrm{P}_1}} + (1-f) Q_{\mathrm{P}_2} \frac{\overline{\lambda}_{\mathrm{L,UV}}}{\overline{\lambda}_{\mathrm{P}_2}} \right] \tag{7}$$

These formulas can be used to evaluate the conversion losses between pumping with a blue and an ultraviolet LED. Note that in the case of more than one phosphor, absorption of the emission from the short wavelength phosphor by the long wavelength phosphor(s) is not taken into account. For the combination of a blue LED with YAG:Ce^{3+}, a typical value of 0.33 for *f* is needed, when white light with relatively high color temperature of 5600K is aimed for. Taking 90% quantum efficiency for the conversion phosphor [45], one finds

$$\eta_{\mathrm{e-o,B}} = 0.81 \eta_{\mathrm{L,B}} \tag{8}$$

Assume we want to obtain a similar emission spectrum by combining an ultraviolet pumping LED (center wavelength of 365nm) with a blue phosphor (Q = 0.9) and the same YAG:Ce^{3+} phosphor (supposing it can as efficiently be excited at 365nm). We then find for the total conversion efficiency

$$\eta_{\mathrm{e-o,UV}} = 0.61 \eta_{\mathrm{L,UV}} \tag{9}$$

If both pumping LEDs are equally efficient in converting electrical to optical power, the optical power emitted by the package *UV* is 25% lower than package *B.* For a pumping LED with peak emission

wavelength of 395nm, the reduction is 18%. These calculations were also performed for other phosphor combinations (using two or more phosphors) and different color temperatures, but they yield similar results, as can be expected intuitively. An important factor determining the overall efficiency of the LED is thus the ratio

$$\overline{\lambda}_L/\overline{\lambda}_P \tag{10}$$

which describes the energy loss during the conversion, irrespective of the quantum efficiency of the phosphor. This ratio has also been named the 'quantum deficit' [46]. Consequently it is advantageous from an efficiency point of view to take pumping LEDs with emission at as long wavelengths as possible.

Hence, what are the advantages of using ultraviolet pumping LEDs compared to blue ones? First of all, if the electrical to optical power conversion is more efficient in UV than in blue LEDs, shifting to UV LEDs can yield an overall more efficient design. Secondly, it is questionable whether good color rendering in combination with a low color temperature can be obtained using a blue LED and a single conversion phosphor. If two phosphor materials have to be used anyway, including one with a small Stokes shift to cover the emission spectrum around 500nm, one might consider the full phosphor approach with ultraviolet pumping LEDs. This also has the advantage that the emission spectrum can be more stable with respect to the driving current and the temperature of the LED chip. In this case, spectral shifts of the pumping LED are not reflected in spectral or intensity changes in the phosphor emission, on condition that the excitation spectrum of the phosphor is sufficiently 'flat' around the emission of the pumping LED. When a blue pumping LED is used, shifts in the emission spectrum of the LED will induce a color shift of the white LED.

Consequently, both approaches seem useful, as long as the peak wavelength of the UV pumping LED is not too short, as this would create too large Stokes losses and an inherently lower electrical-to-optical conversion efficiency of the device.

4. Phosphor requirements.

4.1. Emission spectrum.

Upon developing a white LED, one should first establish the type of light source one is aiming at. Generally spoken, a high color rendering requires having emission over a large part of the visible spectrum. This goes at the cost of efficiency, and vice versa: very high efficiency can be obtained from suitable (quasi)monochromatic sources. Obtaining high color rendering or high efficiency is not entirely mutually exclusive, as will be shown further on.

Fig. 4 shows the CQS and LER for a combination of three hypothetical light sources, characterized by Gaussian-shaped emission bands and a full width at half maximum (FWHM) of 10nm. The peak emission wavelength of the first (blue) light source was fixed at 460nm, as a compromise between sufficient short wavelength emission and still reasonable eye sensitivity. This choice is motivated by the fact that the eye sensitivity drops significantly at shorter wavelengths and 460 nm is by far the most common peak wavelength of blue LEDs, and also the wavelength of the ubiquitous white LEDs based on conversion by YAG:Ce. The peak emission wavelength of the two other light sources was varied over the range from 510nm to 570nm and 580nm to 700nm, respectively. For each combination, the intensity of the three light sources was varied to obtain a white light source with a CCT of 3000K (warm-white light, ready to replace incandescent light sources) and without deviation from the black body locus (duv = 0). The CQS value (which is an optimization of the color rendering index (CRI)) and the LER (luminous efficacy of the radiation) were determined for each distribution [25]. The same was repeated for white light with a CCT of 4500K (Fig. 5).

For a CCT of 3000K, choosing the green light source in the region from 530 to 545nm and the red one from 605 to 615nm, leads to a rather narrow region where the CQS attains a value of 70, which is barely acceptable for general lighting applications. Within the mentioned region, a LER value of 400 lum/W can be obtained, which is about the highest value that can be obtained for a white light source. For a CCT of 4500K, basically the same results are obtained with a similar CQS and only slightly lower LER, due to the relatively stronger contribution of the blue emission line, for which the eye is less sensitive. As will be discussed in section 5.1.2, these narrow emission bands nicely simulate the emission of several trivalent rare earth elements showing 4f-4f emission lines (e.g. Tb^{3+} at 540nm and Eu^{3+} at 615nm).

As apparently, a sufficiently good color rendering cannot be achieved with a small number of narrow emission peaks, the use of 4f-4f line emitters seems less suited for high color rendering lighting applications. However, the LER values can be high, which would for instance make them an ideal choice for display applications, such as liquid crystal displays (LCDs), where LEDs can be used as backlights. In this case only the color saturation of the primary colors is important.

Clearly, with three narrow light sources no decent color rendering can be obtained. Ideally, the CQS should well be into the high 80s or in the low 90s. Therefore we simulated as a second case three hypothetical light sources, with a FWHM of 30nm (blue), 50nm (green) and 70nm (red). These are realistic values for Eu^{2+} doped phosphors. This model is also applicable to blue LED pumped white LEDs, as the FWHM of a blue LED is typically close to 30nm.

With these broader emission bands, a CQS of more than 90 can easily be obtained, in combination with a LER of 300 lum/W, when the green emission band is centered at 525nm and with the red one

peaking at 610nm. Furthermore, there exists a relatively large area where the CQS is above 85, which allows variations in the exact peak position and shape of the phosphors' emission bands.

When using even broader bands, a CQS of (nearly) 100 can be obtained, but this comes at the expense of efficiency, as more photons are emitted at the extremes of the visible spectrum, where the eye sensitivity is lower. Nevertheless it is possible to construct an emission spectrum with high CQS values (>95) in combination with a LER of 250lum/W.

Running the same analysis with a FWHM of 30nm for all three light sources leads to a maximum value of the CQS (and CRI) in the low 80s and to a LER of up to 350lum/W. Hence smart light sources based on three LEDs can yield white light with sufficient color rendering for several applications. If however high color rendering is required, the addition of a fourth LED is required.

Remark that a similar calculation on the relation between emission wavelengths and color rendering was performed in a recent review [4]. However, in this case only narrowband (line) emitters were considered. Also the traditional CRI colour rendering index was used, which is known to be insufficiently accurate to describe narrowband sources. It is easy to see that color reproduction with narrowband sources can critically depend on the exact emission wavelengths for samples having a rapidly changing reflectance spectrum. For example, tomatoes are notoriously difficult to faithfully visualize in this respect.

If 'good' phosphors are available, light sources with different color temperatures can be achieved by simply changing the weight ratio between the different phosphors (and also the total loading in the case of a blue pumping LED) [47]. This can be understood by observing that there is a relatively large cross-section between Fig. 6 and Fig. 7 for the regions with high color rendering, as simulated for CCTs of 3000 and 4500K.

Of course not all (white) LEDs are being used for general lighting purposes. For instance, they have already entered the market as backlights for liquid crystal displays replacing fluorescent lamps. In this case, these LEDs should contain a significant emission in the blue, green and red part of the emission spectrum, such that after filtering bright and saturated colors are retained. In this case, color temperature, color rendering and deviation from the black body locus are less important parameters. Xie *et al.* proposed a two phosphor-conversion approach for backlight purposes (using a blue LED in combination with green emitting β-sialon:Eu^{2+} (FWHM of 55nm) and red emitting $CaAlSiN_3:Eu^{2+}$) to arrive at color gamut of 92% for the NTSC standard [48].

4.2. Excitation spectrum.

Proper combination of high-performance phosphors is obviously required to obtain a light source with high efficiency and decent emission color properties. A second important criterion in the usefulness of phosphors is related to the excitability of the phosphors, i.e. how well do their excitation spectra match with the emission of the pumping LEDs. Indeed, this is the main reason why the – fully optimized – fluorescent lamp phosphors are in most cases useless for application in LEDs. These phosphors are mainly excited by the 254nm emission line of mercury. For reasons of energy efficiency, it is not desirable to develop pumping LEDs with emission in this wavelength range.

Hence phosphors with good excitability in the near-UV to blue region of the spectrum are required. Furthermore, the excitation spectrum should be sufficiently broad to compensate for changes in the emission spectrum of the pumping LED, caused by changes in the driving current and/or the junction temperature. To keep color stability for the entire wLED, it is therefore advisable to have a relatively flat excitation spectrum for the phosphor near the peak emission of the LED.

This puts some restrictions on the type of dopants which can be used. The rare earth line emitters, such as Eu^{3+}, Tb^{3+}, Sm^{3+} and Pr^{3+} have in general only narrow 4f-4f excitation lines in the near-UV to blue part of the spectrum. Charge transfer states (CTS) and 5d levels are generally situated at higher energies, which are for instance available in fluorescent lamps, as mentioned earlier. For instance, Eu^{3+} has excitation lines around 394nm and 465nm, which at first glance is interesting for pumping. However, the width of the lines in the excitation spectrum is often much narrower than the pumping LED, thus lowering the overall conversion efficiency. This is especially problematic in the case of near-UV pumping LEDs, for which all emitted photons should be converted. Furthermore, slight temperature or current dependent shifts in the emission spectrum of the LED can thus lead to changes in the light output of the phosphor, due to changes in the spectral overlap. Also, changes in the phosphor's excitation spectrum can modify the overlap with the emission of the LED. For instance, $La_2O_2S:Eu^{3+}$ has been reported to have a 60% higher light output at 120°C compared to room temperature when pumped at 405nm, which is at the edge of the charge transfer excitation band and not coinciding with internal 4f-4f transitions of Eu^{3+} [49]. Thermal broadening of this band increases the overlap with the excitation source, and thus leads to an increased light output, counteracting the 'normal' thermal quenching behavior.

Therefore, the broad band emitting rare earth ions (Eu^{2+} and Ce^{3+}) are a more logical choice as their excitation spectrum is also composed of relatively broad bands. Also (sensitized) Mn^{2+} can be a good option. In general, the Eu^{2+} excitation spectrum is somewhat broader and flatter than the one for Ce^{3+}, due to the large splitting of the $4f^6$ multiplet in Eu^{2+}. At higher temperature, the absorption strength of Ce^{3+} somewhat reduces, due to a thermal population of the higher Stark levels of the $4f(^2F_{5/2})$ ground state, from which the transition to the lower 5d excited state is symmetry forbidden [45].

Besides spectral changes in the LED's emission spectrum as a function of junction temperature, also the emission properties of the phosphor can be influenced by temperature, as will be discussed in the next section.

4.3. Thermal behavior.

When the conversion phosphor is situated in close proximity of the LED chip, its thermal behavior is of great importance. Indeed, for a high-power LED of 5W (electrical input power) with an overall efficiency of 150lum/W, approximately 40% of the input power is converted to optical power while 3W of heat has to be dissipated by the device. The losses are obviously related to non-radiative recombination in the pumping LED, the Stokes losses of the phosphor and non-radiative decay in the phosphor. Given the small chip area and the limited phosphor area, heat management is an important issue in the LED design. Nevertheless, temperatures of 400 to 450K can be reached near the LED chip. As a consequence, the phosphor should maintain its quantum efficiency and spectral characteristics at these elevated temperatures. The former is determined by the thermal quenching of the total emission intensity. For the latter, shifting and/or broadening of the emission spectrum can alter the emission color (both CCT and duv) of the entire device. Also, the excitation spectrum can change, thus influencing the absorbed fraction of the emission of the pumping LED. Consequently, a phosphor evaluation should at least contain a study of the thermal quenching behavior, i.e. the variation of the emission intensity (or, ideally, the quantum efficiency). In first order, the decay time of the luminescence is following a similar thermal behavior than the intensity quenching (Fig. 8) [50].

Preferably, also the emission and excitation spectra should be reported as a function of temperature. Upon increasing temperature, the emission spectrum of Eu^{2+} and Ce^{3+} broadens due to the occupation of higher vibrational levels. In addition, changes in the peak emission position are possible. For the 4f-4f emitting rare earth ions, spectral shifts and thermal broadening of the emission spectrum are largely negligible.

Several non-radiative decay paths are determining the thermal quenching of the (integrated) emission intensity. In general, the thermal quenching behavior is explained in the configurational coordinate diagram, where thermally assisted crossing between the energy parabola of the excited and the ground state leads to non-radiative decay. This also implies that for a large Stokes shift (i.e. when the equilibrium position of the excited state strongly differs from the one for the ground state), thermal quenching will appear at lower temperature. As pointed out by Dorenbos, this simple model does not accurately describe the thermal quenching in the 5d-4f emitters, such as Eu^{2+}. For these ions the (thermally assisted) auto-ionization of the luminescent ion leads to thermal quenching, which is strongly related to the proximity of the 5d excited states to the bottom of the conduction band [51].

For the f-f emitters, another quenching mechanism takes place as the Stokes shift between ground and excited 4f state is negligible for these ions. The quenching then takes place via the phonon-activated crossing of the excited state and the charge transfer state [52] or by multi-phonon emission [53].

4.4. Quantum efficiency.

When designing LEDs, one should not only focus on the shape of the emission spectrum, but give equal attention to the efficiency of the entire conversion process of electrical power to the observed optical power. To obtain such a high efficiency, using phosphors with quantum efficiency close to unity is of the utmost importance. Many reports on new LED conversion phosphors do not mention the quantum efficiency at all. In principle, measuring the (internal) quantum yield is relatively straightforward:

$$\begin{aligned} n_{\mathrm{exc}} &= n_{\mathrm{refl}} + n_{\mathrm{conv}} + n_{\mathrm{n-r}} && (11) \\ &= n_{\mathrm{refl}} + Q n_{\mathrm{abs}} + (1-Q) n_{\mathrm{abs}} && (12) \end{aligned}$$

Here n_{exc} is the number of photons directed towards the phosphor, n_{refl} contains the number of reflected photons, n_{conv} is the number of emitted photons by the phosphor and $n_{n\text{-}r}$ comprises all photons lost in non-radiative transitions. The quantum yield is the ratio between converted and absorbed photons and can be determined as follows

$$Q = \frac{n_{\mathrm{conv}}}{n_{\mathrm{abs}}} = \frac{n_{\mathrm{conv}}}{n_{\mathrm{exc}} - n_{\mathrm{refl}}} \qquad (13)$$

If an absolute measurement of the quantum efficiency is not possible, then one should at least compare it to a well-established conversion phosphor, showing similar excitation behavior. Obviously, during comparison the integrated emission intensities should be compared, and not the peak emission intensities. This is especially true when comparing line emitters (such as Eu^{3+}) to broad-band emitters (such as Eu^{2+} or Ce^{3+}) [54]. Ideally, the same excitation wavelength should be used, to eliminate (uncorrected) differences in excitation flux inherent to most excitation light sources.

Ideally the quantum efficiency should approach unity, to maximize the overall efficiency of the lighting devices. YAG:Ce^{3+} has a quantum efficiency well above 0.9 [45], which makes it a tough target value for other, alternative, phosphors. Obviously, reporting the quantum efficiency at room temperature should be done in conjecture with the thermal quenching behavior. In this way, one can fully assess the phosphors performance upon device incorporation.

Up to this point in this work, the term 'quantum efficiency' was used to describe the *internal* quantum efficiency, i.e. the ratio between the number of emitted photons and the number of absorbed photons, which is an intrinsic property of the luminescence conversion process.

To assess a specific phosphor when incorporated in an LED device, the *external* quantum efficiency should also be considered. This is the ratio between the number of emitted photons and the number of incident photons, or differently, the internal quantum efficiency times the absorbed fraction of the excitation light. In general, increasing the dopant concentration in a phosphor increases the absorption at the excitation wavelength. However, there exists a trade-off between the increasing absorption (and emission) and a decrease in the internal quantum efficiency due to concentration quenching. For application in LEDs, using a phosphor with a high external quantum efficiency allows to use a low amount of phosphor material on the LED chip. This limits the absorption losses of the down-converted light. Therefore it is advantageous to have dopant ions with high absorption cross section, such as Eu^{2+} and Ce^{3+}, in contrast to for instance line-emitting rare earth ions which have low absorption strengths for the 4f-4f transitions.

In a real phosphor material, for instance being composed of coarse grains, scattering of the down-converted light will lead to increased absorption losses, thus lowering the total number of photons extracted from the phosphor layer. Scattering losses will thus be determined by the particle size and their distribution. Also, broad particle size distribution can lead to inhomogeneous emission colors. Obviously these parameters are important when fabricating commercial devices; however, they are

practical issues determined by the synthesis method (and possible post-synthesis treatments). Therefore, in this work, we will focus on the intrinsic property of the conversion process, although for some phosphor materials it is still a challenge to get specific and narrow size distributions [55].

4.5. Stability.

Current commercially available products mention lifetimes typically from 15,000 to 50,000 hours. The latter corresponds to more than 20 years of operation for 6 hours per day. This leads to stringent lifetime requirements on the packaging, the color conversion material and the driver electronics.

In the early days, wLEDs suffered from yellowing of the epoxy material [37, 56], thus altering the emission color and lowering the light output. The use of thermally and UV-resistant encapsulating materials remediated this problem. Of course, in the case of UV-pumping LEDs, special attention is required on the choice of packaging material. The color conversion material itself should also be as stable as possible. Especially for several sulfide-based phosphors (such as CaS:Eu and SrS:Eu) problems have been reported, as these materials are not stable in ambient air. Contact with moisture leads to an irreversible degradation of the phosphor, a reduced light conversion and thus a shift in emission color. Also, development of corrosive H_2S during degradation can further reduce the light output of wLEDs, due to a decreased reflectivity of Ag-coated cups and contact pads [57]. Although encapsulation of sulfide phosphors by an oxide coating improves the resistance against hydrolysis (Fig. 9) [58-60], the use of intrinsically stable phosphor materials (such as oxides or (oxy)nitrides) is preferred.

4.6. Saturation effects.

Saturation effects in phosphor-converted LEDs should not be underestimated for some dopant ions with long decay times. Saturation is defined here as a sub-linear increase of the light output for

increasing excitation intensity. When the phosphor material is positioned close to the LED chip, it should be able to convert high photon intensity. The continuous increase in the efficiency of the pumping LEDs further increases the photon flux for a similar chip size. If a color conversion material with a long decay time is used, the light output at high excitation flux can be lower than the value extrapolated from the low-power performance. This has been observed for Mn^{2+} (decay time of several to tens of ms) [61, 62], which was related to ground-state depletion (thus lowering the absorption strength) or to energy transfer between dopant ions in the excited state [61]. Interestingly, in co-doped Eu^{2+}-Mn^{2+} phosphors a sub-linear response was observed for both the Eu^{2+} and the Mn^{2+} emission, due to an increased energy transfer from Eu^{2+} to Mn^{2+}, when Mn^{2+} was in the excited state compared to it being in the ground state [63]. Fig. 10 shows the normalized emission spectra for a white LED package (based on a UV pumping LED) as a function of the driving current. The blue and green phosphors ($Sr_2Ga_2SiO_7$:Eu^{2+} and $Sr_5(PO_4)_3Cl$:Eu^{2+} do not show any conversion saturation, while the red emission from $(Sr_{0.76},Ca_{0.1})_2P_2O_7$:$0.02Eu^{2+}$,$0.10Mn^{2+}$ shows a strong saturation, leading to color shifts upon variation of the driving current [64].

Different packaging, with a remote phosphor layer, can prevent these effects by reducing the excitation density. For the broadband emitting ions Eu^{2+} and Ce^{3+} no saturation is expected, due to the much shorter decay time, in the range of hundreds and tens of nanoseconds, respectively [65, 66]. For several 4f-4f line emitters, like Eu^{3+} and Tb^{3+}, the decay time is typically a few ms [67], therefore saturation effects are also possible in this case.

4.7. Overall evaluation of usefulness.

The six abovementioned parameters should all be evaluated, as failure in one aspect in principle renders the phosphors useless for commercial applications. Often, one evaluates a (new) phosphor by studying its luminescence properties in dedicated fluorescence spectrometers. While this is of

course very interesting from a fundamental point of view, care must be taken to assess these properties in conditions mimicking the pumping LEDs behavior. For instance, upon determination of the emission spectrum and the quantum efficiency, a monochromatic excitation source (i.e. having a very narrow spectral distribution) is often used. In a real LED-phosphor combination however, the results can differ considerably, due to a reduction in the absorption efficiency of the phosphor for other than the peak wavelength of the LED's emission.

Ideally, the phosphor should be evaluated in conjecture with its pumping LED, where one then carefully measures the global emission spectrum, color properties (CRI or CQS, CCT, duv) and luminous efficiency of the entire device (in lumen per watt *electrical* input power) as a function of driving current and temperature. Of course, this requires the know-how to prepare phosphor coated devices in order to obtain reproducible results.

5. Choice of phosphors and current status.

Some of the abovementioned six requirements are primarily related to the properties of the dopant ions (such as the shape of the emission band), while others are influenced by the composition of the host material, such as the chemical and thermal stability. Several other requirements are related to the interplay between host and dopant, such as the thermal quenching behavior. Therefore, it is not straightforward to propose ideal combinations of host and dopant(s). In this section, we will nevertheless discuss generically the choice of the dopant ion and several classes of host materials.

Table 2 shows key parameters for a selection of LED phosphors, for which thermal quenching behavior and quantum efficiency were reported.

Table 2. Key parameters for a selection of LED phosphors: peak emission wavelength (λ_{em}), quenching temperature $T_{0.5}$ (temperature for which the integrated emission intensity is half of that at low temperature), emission intensity at the specified temperature compared to room temperature (I/I_{RT}), internal and external quantum efficiencies (QE).

Host	Dopant	Conc (%)	λ_{em}(nm)	$T_{0.5}$(K)	I/I_{RT} (%) at T(K)	QE (int/ext)	Ref
$Y_3Al_5O_{12}$	Ce^{3+}	0.033	536	>700	95, 450	>90/-	[45]
		3.33	558	525	77, 450	81/-	[45]
$Ca_{0.8}Sr_{0.2}S$	Eu^{2+}	1	635	400	70, 420	51/47	[68]
Ca_2SiS_4	Eu^{2+}	2	660	460	90, 420	-/35	[69, 70]
$SrGa_2S_4$	Eu^{2+}	0.1	537	470	-	57/-	[71, 72]
Sr_3SiO_5	Eu^{2+}	7	568	400	-	-/68	[51, 73]
$BaMgAl_{10}O_{17}$	Eu^{2+}	11.6	450	-	90, 425	92/-	[49, 74]
Li_2SrSiO_4	Ce^{3+}	3	442	-	92, 450	81/57	[75]
Sr_2BaAlO_4F	Ce^{3+}	3	502	-	50, 500	93/-	[76]
$Ca_2Si_5N_8$	Eu^{2+}	2	605	-	40, 450	55/-	[77]
$Sr_2Si_5N_8$	Eu^{2+}	2	622	-	86, 450	80/64	[78]
$Ba_2Si_5N_8$	Eu^{2+}	2	570	530	78,450	75-80/-	[77, 79]
$BaYSi_4N_7$	Eu^{2+}	1	520	-	15, 475	16/11	[80]
$CaAlSiN_3$	Eu^{2+}	0.8	650	-	65, 450	80/70	[81]
		8	666	-	87, 450	91/73	[78]
	Ce^{3+}	1	580	-	84, 450	80/56	[82]
$SrAlSiN_3$	Eu^{2+}	0.8	610	-	70, 450	80/70	[81]
$SrYSi_4N_7$	Eu^{2+}	1	534	-	30, 475	26/19	[80]
AlN	Eu^{2+}		465	-	90, 450	73/46	[83]
$CaSi_2O_2N_2$	Eu^{2+}	2	560	600	-	76/-	[50]
$SrSi_2O_2N_2$	Eu^{2+}	2	537	600	-	91/-	[50]
$BaSi_2O_2N_2$	Eu^{2+}	4	495	-	84, 450	65/51	[78]

		2	494	440	-	71/-	[50]
$Ba_3Si_6O_{12}N_2$	Eu^{2+}		530	-	90, 400	-	[84]
α-SiAlON	Yb^{2+}	0.5	550	-	74, 450	58/26	[78]
α-SiAlON	Eu^{2+}	7	567	-	88, 450	71/88	[78]
β-SiAlON	Eu^{2+}	0.3	536	-	85, 450	49/33	[78]
Ca-α-SiAlON	Eu^{2+}	5	580	-	85, 450	-/44	[85]
Li-α-SiAlON	Eu^{2+}	7	573	-	-	57/40	[86]

5.1. Choice of dopant ion

5.1.1. Broad band emitting rare earth ions.

When looking at the data compiled in table 2, it is clear that the broad band emitting rare earth ions Eu^{2+} and Ce^{3+} have been widely studied. This is primarily because of their unique emission properties, combining a broad emission spectrum (leading to good color rendering properties), relatively small Stokes shift (allowing excitation in the near-UV or blue part of the spectrum) and short decay times (avoiding saturation). Depending on the host material, high quantum efficiencies in combination with a good thermal quenching behavior can be obtained. Furthermore, the emission spectrum can be tuned from the near-UV to deep red, by appropriately choosing the host compound (section 5.2).

The effect of the host on the luminescence properties of Ce^{3+} is indicated in Fig. 11. The 4f ground state shows a spin orbit splitting into two levels ($^2F_{5/2}$ and $^2F_{7/2}$), with an energy separation of about 2000cm^{-1}.Compared to the free (gaseous) Ce^{3+} ion, the lowest 5d excited state is decreased in

energy, or red-shifted, upon incorporation in an inorganic compound. This red-shift is composed of the centroid shift (resulting from the nephelauxetic effect, determined by the polarizability of the surrounding anions) and the crystal field splitting (determined by the shape and the size of the first anion coordination polyhedron) [87]. Hence by variation of the composition of the host material, the emission and excitation wavelength can be changed. Upon excitation of the 4f electron to the 5d orbital, lattice relaxation occurs (the same kind of relaxation occurs after the transition to the ground state), which leads to the Stokes shift, being the difference between the absorption and the emission energy. For Ce^{3+}, a broad emission spectrum is obtained due to the transitions from the 5d excited state to the spin orbit split ground state.

Upon doping with Eu^{2+} a similar figure can be drawn, with the main difference that the $4f^7$ ground state is a single level ($^8S_{7/2}$), i.e. no spin orbit splitting is present and the emission spectrum is in principle characterized by a single emission band, with a typical FWHM in the range from 50 to 100nm [87]. In some compounds, multiple emission bands are present, which can lead to a broadening of the emission spectrum. This effect is observed in cases where the Eu-ions are incorporated on lattice sites with different symmetry and/or a clearly different distance with the nearest neighbor ions. In general Eu^{2+} emission can be observed when the Eu^{2+} is either at a monovalent or a divalent cation site. Apart from a few exceptions, Eu^{2+} emission is not observed when substituting for a trivalent ion, due to the 5d excited state being situated in the host's conduction band [87]. In AlN, Eu^{2+} emission at 470nm is observed upon co-doping with Si [88], while the incorporation of O^{2-} in $LaSi_3N_5$:Eu leads to broadband Eu^{2+} emission at 549nm [89].

Often, Eu^{2+} ions are substituting for divalent alkaline earth ions, such as Mg^{2+}, Ca^{2+}, Sr^{2+} and Ba^{2+}, thus requiring no charge compensation. As the ionic radius of Eu^{2+} is very similar to the one for Sr^{2+}, high dopant concentrations can be substitutionally doped into Sr-based host lattices without the formation of europium-rich precipitates. For alkaline earth ions with a smaller ionic radius, such as

Ca^{2+}, Eu-clustering has been observed at higher concentrations [90]. In combination with this large solubility, the shape and position of the emission spectrum is roughly independent of the dopant concentration for most of the Eu^{2+} doped compounds, provided that the crystallographic phase of the undoped host is maintained upon doping. Depending on the value of the Stokes shift, reabsorption can become prominent at elevated doping concentrations, leading to a red-shift of the emission spectrum.

In contrast to the binary sulfides, which show relatively strong concentration quenching [68, 90], the ideal dopant concentration in ternary and multinary compounds can be relatively high, up to 10 to 20% substitution, in combination with strong absorption bands caused by the dopant. Fig. 12 shows the diffuse reflection spectra for $Sr_{2-x}Eu_xSi_5N_8$ [77]. Remark that these very high dopant concentrations can lead to a prohibitive cost of the phosphor material, due to the elevated price of Eu.

The excitation spectrum for Eu^{2+} doped compounds is broad and often relatively featureless, due to the splitting of the 5d excited state by the crystal field, coupling to the multiplet splitting of the $4f^6$ configuration. The latter is similar to the ground state splitting for the ^7F_J levels of Eu^{3+}, which sometimes leads to a staircase-like fine-structure in the excitation spectra [91]. For green to red emitting phosphors, an excellent overlap is possible with both near-UV and blue pumping LEDs.

The emission spectrum of Ce^{3+} is blue-shifted compared to that of Eu^{2+} when doping in the same compound [92]. It is also intrinsically broader than the one for Eu^{2+}, due to the additional spin orbit splitting (about $2000cm^{-1}$) of the $4f^1$ ground state (Figs. 11 and 13). In the case of the yellow-emitting YAG:Ce^{3+}, the broadness of the emission spectrum allows to arrive at a decent color rendering using the combination of a blue pumping LED and a single phosphor.

The excitation spectrum of Ce^{3+} consists of up to five often distinguishable excitation bands due to the crystal field splitting of the excited 5d state. For YAG:Ce^{3+}, where Ce^{3+} experiences a much larger crystal field splitting (~ 27000cm^{-1}) than in most other oxide compounds [93], the two lowest excitation bands at 340nm and 460nm are well separated (Fig. 13), leading to an almost negligible absorption at 390nm [45]. Therefore the emission spectrum of the pumping LED should be chosen such as to nicely match one of these excitation bands of YAG:Ce^{3+}. For elevated Ce^{3+} concentration, the emission spectrum is red-shifted due to reabsorption (Fig. 13) [45, 94].

Ce^{3+} can show luminescence when substituted at both a divalent or trivalent cation site. At the former site, charge compensation is required. This can be provided by intrinsic defects, such as vacancies, but this often leads to more significant concentration quenching, with clustering of Ce^{3+} ions and correlated red shift of the emission spectrum. Codoping with monovalent cations can improve the incorporation in this case, by restoring charge balance [95].

Also divalent ytterbium can show broad band emission due to a $4f^{13}5d – 4f^{14}$ transition [96]. Based on the general behavior of the $4f^n$ and 5d energy level positions in inorganic hosts , the 5d-4f emission energies of Eu^{2+} and Yb^{2+} are expected to be similar within 0.1eV [97, 98]. The thermal quenching is in general more prominent for Yb^{2+}, due to the closer proximity of the 5d excited state to the conduction band compared to Eu^{2+} [97, 99]. Also the relatively long decay time of Yb^{2+} (1-10ms, [98]) could lead to saturation for high excitation flux.

However, in many compounds the emission of Yb^{2+} is absent or considerably red-shifted (showing so-called anomalous emission, with larger Stokes shift and larger emission band width), due to interaction of the 5d excited state with the conduction band levels or the formation of a self-trapped exciton [100, 101]. Although this red-shifted emission appears interesting for LED applications, the

relatively strong thermal quenching for Yb^{2+} doped compounds makes them less suited as conversion phosphors.

5.1.2. Line emitting rare earths.

Most trivalent rare earth ions (with Ce^{3+} as the major exception) yield a set of relatively narrow emission lines, due to internal $4f^n$-$4f^n$ transitions, which are hardly affected by the host compound. The host plays some role though in the emissive properties of these 4f-4f emitters, as it influences the relative strength of the emission lines (via selection rules associated with the local symmetry), the crystal field dependent splitting of the emission lines and the quantum efficiency (through the presence of non-radiative pathways and the thermal quenching behavior).

Several of these rare earth ions yield visible emission. Especially Tb^{3+} (green emission, main peak near 545nm) and Eu^{3+} (orange to red emission, main peak near 600 or 620nm) are interesting rare earth ions, which have extensively shown their usefulness in fluorescent lamp phosphors or cathode ray tubes. As mentioned in section 4.2 the major problem with transferring these materials to LED applications is the lack of efficient, broad band excitation paths in the near-UV to blue part of the spectrum, as 5d levels and charge transfer states (CTS) are generally situated well below 350nm, as illustrated for $Y_2O_2S:Eu^{3+}$ (Fig. 14(a)). For Eu^{3+}-doped $(Sr,Ba)_2CaMoO_6$ however, energy transfer occurs from the MoO_6^{6-} complex, which enables efficient pumping around 400nm (Fig. 14) [102].

The excitation spectrum can also be extended towards longer wavelength by sensitizing through the appropriate addition of co-dopants. For instance, Tb^{3+} emission can be sensitized by the addition of Ce^{3+} [103, 104]. Addition of Bi^{3+} has been reported to create additional (broad band) pathways for Eu^{3+} [105]. We already mentioned that efficient white light emission can be obtained by combining narrow line emission at 460nm, 540nm and 610nm (Fig. 5). In this case wLEDs can be made with

moderate color rendering properties, but with high luminous efficiency. Interestingly, the main emission peaks of Tb^{3+} and Eu^{3+} match the required green and red component. Also, the use of Eu^{3+}-doped red phosphors is advantageous because the reabsorption of the emission of the green phosphor is avoided, which can be a problem for red phosphors based on Eu^{2+}.

Several other rare earth ions with visible luminescence have been studied for LED applications, such as Dy^{3+}, Sm^{3+}, Tm^{3+} and Pr^{3+}. $Dy^{3+}(4f^9)$ shows three emission peaks (485nm, 570nm and a less intense red emission around 660nm) which can in principle lead to white emission, though with a poor color rendering [106]. The red emission of Sm^{3+} ($4f^5$) is characterized by several emission peaks at approximately 560, 600, 650 and 700nm, in combination with a 4f-4f excitation peak around 405nm [107, 108]. The quantum yield is seldom reported (which is often the case for the rare earth line emitters), although it is rather low in heavy metal tellurite glass [107]. Tm^{3+} ($4f^{12}$) has a blue emission peak at 450nm (excitable around 360nm) [109], but the conversion efficiency is lowered by competing infrared emitting decay paths [110]. Pr^{3+} ($4f^2$) has several transitions leading to emission in the visible part of the spectrum, with green emission originating from the $^3P_0$ excited state and red emission from both $^3P_0$ and $^1D_2$ excited states. The relative intensity is strongly dependent on the type of host material [111]. Adding Pr^{3+} to YAG:Ce^{3+} slightly increased the color rendering (due to a dominating emission at 610nm), but strongly reduced the overall efficiency of the phosphor [112]. For these rare earth ions, their apparently limited efficiency, in combination with the lack of broad band excitation in the near-UV and blue, makes them less suited as dopants for LED phosphors.

5.1.3. Other dopants.

Although the largest fraction of the state-of-the-art conversion phosphors is based on the (broad band emitting) rare earth ions, the use of several other types of dopants has been reported, such as the transition elements (e.g. Mn^{2+}, Cr^{3+}, ...) and the s^2 ions (Pb^{2+}, Bi^{3+}, Sb^{3+},...).

Divalent manganese has a d^5 electron configuration, with emission originating from parity-forbidden d-d transitions. Using the Tanabe-Sugano diagrams [113], it can be derived that emission originates from $^4T_1$ to $^6A_1$ transitions. The position of the lowest excited state strongly depends on the crystal field strength, which allows shifting the Mn^{2+} emission from green to red, depending on the host [67, 114]. The emission has typically a FWHM of 60nm, which is narrower than for Eu^{2+} in similar compounds [114, 115]. Two effects are associated with the spin and parity forbidden character of the transition. Firstly, the long decay time for Mn^{2+} (typically being several to tens of ms [67]) inevitably leads to saturation in high flux devices [61, 63]. Secondly, the low absorption strength for the direct excitation of Mn^{2+} hampers its use in LEDs. The absorption can be increased however by energy transfer following host absorption or by using suitable sensitizers. The first way is less suited when using near-UV or blue pumping LEDs. Sensitizing can be achieved by codoping with Eu^{2+} [116, 117], Ce^{3+} [118] or Sb^{3+} [113, 119]. The energy transfer from the sensitizer to the Mn^{2+} centers occurs via exchange interaction, requiring a first neighboring position [63]. Consequently, the emission from the sensitizing ions is in general still present, even for a much larger Mn^{2+} concentration compared to the sensitizer concentration [63]. In principle this could be an advantage, as in this way very broad or even white emission can be obtained, by appropriately choosing the relative dopant concentration [120, 121]. However, especially the temperature dependency should be carefully investigated, to rule out temperature dependent color shifts [122].

Recently, Duan et al. reported strong d-d absorption in CaZnOS:Mn^{2+}, where the spin and parity selection rule is apparently strongly relaxed [114]. This was explained by a deviation from a pure tetrahedral symmetry. Data on the quantum efficiency and temperature quenching is relatively scarce for the recently highlighted Mn^{2+}-doped compounds (Table 2).

Several authors report the use of Cr^{3+}-doped phosphors, to enhance the light output in the (deep) red part of the spectrum [123, 124]. When co-doped in YAG:Ce^{3+}, intense Cr^{3+} emission centered around 700nm could be obtained, enhanced by energy transfer from the Ce^{3+} ions [123]. The practical use of Cr^{3+} for white LEDs is however very limited, given the very low eye sensitivity for these wavelengths. This is also illustrated in Fig. 4 where one observes a strong drop in the LER of a white light source when the peak wavelength for the red emission is situated beyond 650nm.

A final class of dopant ions consists of the so-called s^2 ions, such as Sn^{2+}, Pb^{2+}, Bi^{3+} and Sb^{3+}, which show luminescence due to a transition from an nsnp to an ns^2 electronic configuration. These luminescence ions have been in the picture for other applications, e.g. as fluorescent lamp phosphor, with $Ca_5(PO_4)_3(F,Cl):Sb^{3+},Mn^{2+}$ as a well-known white-light emitting lamp phosphor [113, 119]. Most ns^2-based phosphors lack efficient excitation bands in the blue or near-UV part of the spectrum, which probably explains why they are hardly investigated as LED phosphor. Bi^{3+} has however been studied to some extent as sensitizer ion, especially in combination with Eu^{3+} [105]. Recently some reports were published on borophosphates and borates activated with Bi^{2+}, having a $6s^26p$ electronic ground state configuration [125, 126]. Several excitation paths in the near-UV or blue are available, although they are parity-forbidden.

5.2. Choice of host material

From the previous section it is clear that several dopant ions are available to realize high-performance conversion phosphors, depending on the type of emission spectrum aimed for.

The host lattice should also fulfill certain requirements. Obviously, the host material has to be a thermally and chemically stable compound to resist the elevated temperatures near the pumping

LED chip and to realize the long lifetime which makes LEDs truly unique. Also, the material should be optically transparent for the emitted light. Unless a host-dopant energy transfer occurs, the host should also be transparent for the emission of the pumping LED, limiting the choice to wide band-gap materials. Dopants have to be incorporated in the host material, which is facilitated if there is no charge or size mismatch between the dopant ion and the substituted ion in the host. Finally, the phosphor production process should also be cheap and last but not least environmentally friendly, with respect to thermal input and the gasses and precursors used.

It would require a tedious effort to use a simple combinatorial approach for selecting the 'ideal' host-dopant combination, especially because the impact of the composition of the host material on the luminescence properties is rather strong for certain dopant ions (e.g. the broad band emitting rare earth ions and Mn^{2+}). For example, Dorenbos listed the luminescence properties (band width, absorption and emission energy) for more than 300 Eu^{2+}-doped compounds [87], effectively showing that the emission can be tuned from the near UV to the deep red. Fig. 15 shows the emission wavelength for Eu^{2+} on divalent and monovalent cation sites [87]. Data on recently reported Eu^{2+}-doped (oxy)nitrides were added as well, in the case of low dopant concentration.

Nevertheless, the emission in many compounds is absent or shows an unusual behavior, such as a long decay time, broadened and red-shifted emission (the so-called anomalous emission [97]), again showing the strong influence of the host matrix. However, by modeling the influence of the host's band gap and the local environment for the rare earth dopants (symmetry, distance and type of ions in the first coordination shell) it is possible to predict up to a certain extent the emission properties of certain host-dopant combinations, such as the thermal quenching behavior [51] and the position of the rare earth 4f and 5d levels with respect to the host's band gap [127].

Recently, several review articles have been published on specific classes of host materials for LED phosphors (such as the (oxy)nitrides [55, 128], sulfides [129], ...) listing and discussing the different host compounds and their synthesis techniques. Therefore, we will here only discuss the largest 'classes' of host materials in a generic way, focusing on their characteristic properties.

5.2.1. YAG:Ce and its modifications.

The first host compound discussed is – obviously - the well-known yttrium aluminium garnet ($Y_3Al_5O_{12}$, YAG), partly because of historical reasons, partly due to it being the workhorse of high-efficient, cool-white phosphor-converted LEDs till this date. A YAG:Ce^{3+}-based phosphor was used to produce the first phosphor-converted white LED [130], employing the blue InGaN LED as developed by Nakamura [131]. YAG:Ce^{3+} was initially introduced by Blasse and Bril as phosphor for flying-spot cathode ray tubes, due to its short decay time [132] and for similar reasons also studied as scintillation phosphor [83].

An excellent overview of the (temperature dependent) emission properties of YAG:Ce^{3+} can be found in [45], while the different synthesis methods are discussed in [128]. Here we evaluate YAG:Ce^{3+} against the six requirements for conversion phosphors we put forward in section 4:

1. YAG:Ce^{3+} has a very broad emission spectrum with a FWHM of typically 100nm, due to the spin-orbit split ground state of Ce^{3+} (Fig. 11). Its yellow emission color in combination with part of the blue emission from the pumping LED yields white light in the higher CCT range. The color rendering is moderate, although fair enough for backlighting and lighting conditions where color rendering is not so important.
2. YAG:Ce^{3+} can easily be excited by the blue pumping LED, with a sufficiently broad excitation band near 460nm showing good overlap with the LED's emission spectrum. The spin-allowed,

parity-allowed 4f-5d absorption leads to high absorption strength. Also, the optimum dopant concentration can be relatively high (about 5%) before concentration quenching sets in [45, 133].

3. YAG:Ce^{3+} has an excellent thermal quenching behavior, maintaining more than 50% of the room temperature emission intensity at 700K [45], at least for low dopant concentration. For higher dopant concentration, the thermal quenching worsens, although it still outperforms many other phosphor materials. Also, the emission spectrum does not show significant changes at higher temperature, apart from some inevitable broadening.
4. It is characterized by high quantum efficiency (90% and more), imperative for the production of efficient LED packages.
5. It shows an excellent chemical stability and it shows no deterioration under high excitation fluxes encountered in pcLEDs [37, 134].
6. Due to the allowed nature of the emission transition in Ce^{3+}, the emission is fast, with a decay constant of 63ns [45]. Saturation of the conversion process can thus totally be ruled out.

Obviously, YAG:Ce^{3+} receives high scores on all six requirements. The main drawback of YAG:Ce^{3+} lies in the lack of emission in the red part of the visible spectrum, which hampers the development of LEDs with high color rendering and/or low color temperature. The emission spectrum can be red-shifted by introducing Gd^{3+} or Tb^{3+} [135, 136], while substituting (part of the) Al^{3+} by Ga^{3+} leads to a blue-shift of the emission spectrum [137]. In general, these modified YAG:Ce phosphors show a lower thermal quenching temperature. Substitution of Al^{3+} by a combination of $Mg^{2+}$and Si^{4+} leads to a considerable shift of the emission maximum to 600nm, allowing the fabrication of a warm-white LED with relatively high color rendering [138, 139]. The broadness of the emission spectrum, however, also leads to a considerable fraction of the light being emitted beyond 650nm. As the sensitivity of the eye is very low in this part of the spectrum, the overall efficiency of the pcLED is

lowered. Therefore, it would be more efficient to add a second, relatively narrow-emitting red phosphor in the phosphor blend.

For higher Ce^{3+} concentrations, the emission also shows a (small) red-shift, partially due to reabsorption, along with a reduction of the thermal quenching temperature [45]. For high flux devices, the use of lower dopant concentrations is thus advantageous. The associated lower absorption strength can be counteracted by using translucent ceramic plates as color conversion layer, thus strongly reducing scattering losses [45]. Using pre-characterized ceramic sheets [140], which are then transferred onto the blue-emitting LED chip, strongly reduces the binning spread (in emission color) compared to the use of phosphor particles deposited in a resin (Fig. 16).

5.2.2. Sulfides and oxysulfides.

Sulfide hosts, when doped with Eu^{2+}, have been in the picture since the early days of phosphor-converted LEDs, because the emission is – in general - red-shifted compared to their oxide counterparts, mainly due to a larger centroid shift (Fig. 15). A detailed overview of sulfide phosphors and their uses (including that as color conversion phosphor) can be found in [129].

The emission bands of Eu^{2+} in SrS and CaS show broad band emission peaking near 620 nm and 660nm, respectively, in combination with a FWHM of typically 70nm, which is rather well suited for use as red component in white light LEDs [68]. By using solid solutions $Ca_{1-x}Sr_xS:Eu^{2+}$ the emission can be tuned from orange-red to saturated red. Although it has been used in commercial white LEDs, this class of materials shows several drawbacks, such as a relatively strong concentration quenching [141] and a limited stability upon contact with moisture [58]. Also the thermal quenching is rather strong, especially for Sr-rich compounds and for higher Eu-concentrations. Even near room temperature, thermal quenching is already significant [68]. Solid state reactions routes for sulfides often require

toxic H_2S gas, although low-temperature solvothermal synthesis routes are also available [142], yielding sub-micron-sized single crystals [143].

Several ternary sulfide compounds have also been proposed as LED phosphor, with especially the thiogallates receiving some attention due to much better stability than for instance the thioaluminates (in casu green-emitting $SrGa_2S_4:Eu^{2+}$ [37, 38, 71]). For the M_2SiS_4 thiosilicate phosphors, the emission can be changed from deep-blue (Ba_2SiS_4:Ce) to saturated red (Ca_2SiS_4:Eu) by choosing the alkaline earth ion (Ca, Sr, Ba) and the dopant ion (Ce, Eu) [144]. A drawback is the relatively low thermal quenching temperature, typically in the 400 to 450K range.

Many of the above mentioned sulfide compounds show strong reactivity with atmospheric compounds (moisture, carbon dioxide), deteriorating the phosphor and subsequently lowering the luminescence. Encapsulation of sulfides by inert and optically transparent coatings has been shown to considerably enhance the stability, by a variety of techniques such as non-aqueous sol-gel synthesis or atomic layer deposition [58] (Fig. 9). In principle these techniques are transferable to other moisture-sensitive compounds. Of course, one will rather choose an intrinsically stable material (such as most oxides and nitrides), especially when taking the long lifetime of an LED device into account.

Recently, MZnOS-based phosphors were reported (M = Ca, Ba) , having good thermal and chemical stability [114, 145]. $CaZnOS:Eu^{2+}$ shows red emission centered at 650nm, with a thermal quenching behavior slightly better than $SrS:Eu^{2+}$ [145]. $CaZnOS:Mn^{2+}$ has a relatively narrow emission band at 614nm (FWHM of 50nm) and shows strong Mn^{2+} excitation bands in the 350 to 500nm range [114], which is rather uncommon for Mn^{2+} luminescence (see section 5.1.3).

Another well-known oxysulfide is $Y_2O_2S:Eu^{3+}$, which has served as cathode ray phosphor due to its efficient red emission. It can however not be efficiently excited in the near-UV to blue, as the charge transfer bands are situated below 360nm and the internal 4f-4f absorptions of Eu^{3+} near 395nm or 465nm are weak. Therefore, it is rather unfair to use it as a benchmark phosphor for assessing the performance of other conversion phosphors upon excitation in the near-UV or visible [146].

5.2.3. Oxynitrides and nitrides.

The need for stable and efficient phosphors in the red part of the emission spectrum, which oxides and sulfides cannot easily provide, sparked interest in other types of hosts with large crystal field and/or large centroid shift. Indeed, from the six requirements put forward in this Review, it is clear that the broad-band emitting rare earth ions Eu^{2+} and Ce^{3+} show nearly ideal properties; the remaining task is to find suitable hosts in which the red-shift of the emission is large enough. This feature was found in (oxy)nitride phosphors, which led to intensive research into this new class of materials during the past decade. Before, their luminescence properties were hardly investigated, although these materials were studied for their high thermal and chemical stability, strength and hardness, leading to applications such as abrasives and protective coatings. This led to a firm basic knowledge about the crystallographic structures of many (oxy)nitrides, although the system M-Si-Al-O-N (with M = Li, Ca, Sr, Ba, La) still needs further exploration.

Detailed overviews of the structure and luminescence of europium, cerium and manganese doped (oxy)nitride materials can be found in the Reviews by Ye et al. [128], Xie et al. [55, 147] and He et al. [148].

From Fig. 15 and table 2 it is clear that several nitride compounds doped with Eu^{2+} have their emission peak around 600nm or at longer wavelengths, such as $M_2Si_5N_8$ (M = Ca, Sr or Ba) [77, 115]

and $MAlSiN_3$ (M = Ca or Sr) [48, 81]. On average, the Eu^{2+} emission in oxynitride compounds, such as $MSi_2O_2N_2$, is situated in the green-to-yellow part of the visible spectrum [50]. In 2005, Mueller-Mach demonstrated a white LED, with stable CCT of 3200K and Ra of 89, based on a blue InGaN /GaN LED and two Eu^{2+}-doped (oxy)nitrides (Fig. 17) [40]. In the aforementioned hosts, high quantum efficiencies can be obtained (in combination with elevated doping concentrations for strong absorption) with reasonably high thermal quenching temperatures.

Alkaline earth nitrides can be prepared by solid state reaction, using Si_3N_4 and alkaline earth nitrides or metals [55]. Although this process is suitable for mass production, the reactivity of the alkaline earth compounds requires handling under protective atmosphere. Another disadvantage is the high synthesis temperature. To alleviate this, other techniques were proposed, such as ammothermal synthesis (i.e. a solvothermal synthesis involving supercritical ammonia at high pressure) and a gas reduction and nitridation process (using oxide precursors and a gas mixture of NH_3-CH_4) [55]. Also, using $Si(NH)_2$ instead of Si_3N_4 lowers the reaction temperature due to its higher reactivity **[55].**

In general, the chemical and thermal stability of the (oxy)nitride phosphors is hailed as one of their main advantages over other phosphors, such as the sulfides. Stability studies, with respect to oxidation or the photo-thermal influence of high excitation fluxes by the pumping LED, are however hardly reported. Nevertheless there are some indications of stability issues for certain (oxy)nitride compositions [40, 134]. For instance, it appeared that $(Ca,Sr)AlSiN_3$ was more stable [82] against oxidation than $M_2Si_5N_8$ phosphors, the latter showing considerable degradation of the PL intensity when heated to 573K in air, with the stability depending on the stoichiometry [81].

5.2.4. Other host compounds.

Obviously many other host materials have been proposed recently for color convertors, apart from the garnets, (oxy)sulfides and (oxy)nitrides. Some of these hosts have a history in other applications (such as fluorescent lamps), and are currently being (re)investigated for pcLEDs.

The europium-doped silicates (such as Ca_2SiO_4, Sr_2SiO_4, Ba_2SiO_4 and their solid solutions) are interesting because of the unusually broad emission bands for Eu^{2+} [149], which is due to the existence different lattice sites in the material [150]. $Sr_3SiO_5:Eu^{2+}$ shows a yellow-orange emission, while doping with Ce^{3+} yields greenish-yellow emission [151, 152]. A disadvantage of the silicates is the relatively early onset of thermal quenching [134, 153].

Eu^{3+}-based phosphors, such as $Y_2O_3:Eu^{3+}$, $Y(P,V)O_4:Eu^{3+}$, $Y_2O_2S:Eu^{3+}$ played an important role as red component in cathode ray tube and fluorescent lamp phosphors [67]. However, the lack of broad and strong excitation bands in the blue or near-UV makes them of little use in pcLEDs. Eu^{3+} has also been frequently studied in molybdate and tungstate hosts, because of energy transfer between the MoO_4^{2-}, WO_4^{2-} or MoO_6^{6-} complexes and the rare earth ion (Fig. 14) [154].

5.2.5. Quantum dots and impurity-doped nanoparticles.

Next to the myriad of impurity-doped semiconductors discussed above, where the emission originates from electronic transitions within the impurity ion, semiconductor nanoparticles (or quantum dots, QDs) have also been proposed as color conversion material in LEDs. If they become extremely small (with a diameter of a few nm), quantum confinement can occur with a discretization of the electronic band structure. Compared to the bulk situation, the band gap energy then strongly increases, with the presence of pronounced absorption peaks caused by the discretized energy levels [129].

To obtain efficient photoluminescence, non-radiative decay via surface defect states has to be limited, by passivation of the surface with an organic capping, or the use of an inorganic shell. CdSe is currently by far the most reported type of quantum dot used in combination with blue pumping LEDs [152, 155, 156], due to its relatively high quantum efficiency and the tunability of its emission over the entire visible range. The emission is relatively narrow, with a FWHM of typically 30nm, for quantum dot solutions with a narrow size distribution. In combination with the small Stokes shift, this allows combining of a blue pumping LED and green and red emitting QDs (Fig. 18), without spilling too much emission intensity to the deep-red part of the spectrum, where the eye sensitivity is low. Jang et al. reported a device with 41 lum/W efficiency based on multi-shelled CdSe-based green and red emitting quantum dots for use as backlight in flat panel displays [156]. A final advantage of their small size is the elimination of scattering losses (when compared to conventional phosphors) and the possibility to embed them into translucent matrices [157]. The use of current QDs as color convertors on a large scale is however hampered by several issues: i) Cd-based compounds are hardly acceptable from an environmental point of view and the number of alternative, greener hosts with high quantum efficiency, which is a prime requirement for conversion-based LEDs, is limited. ii) The small Stokes shift also leads to strong reabsorption if QDs are used for both green and red emission. Spatial separation of the QDs has been proposed to partially relieve the reabsorption [155]. iii) Thermal quenching is often quite strong compared to bulk impurity-doped semiconductors, necessitating a remote approach for high flux devices. It has been suggested that the organic capping layer of YAG:Ce nanoparticles can be degraded by the light from a 450 nm pump LED [158].

To reduce reabsorption, nanoparticles doped with impurity ions (such as trivalent rare earths or Mn^{2+}) have also been in the picture [159, 160]. Apart from optical arguments (reduced scattering), it is not a priori obvious what is the advantage of nanoparticles compared to bulk phosphors. The increased band gap might reduce ionization and improve the thermal quenching behavior for some materials. On the other hand, the large surface-to-volume ratio in nanoparticles offers additional

non-radiative decay paths, thus reducing the overall efficiency [159]. For YAG:Ce^{3+} nanoparticles with a size of 7nm, the Ce^{3+} emission is slightly blue-shifted compared to the bulk phosphor, while the emission intensity was halved [158]. It appears that much progress can still be made in the field of impurity-doped nanoparticles. One of the main obstacles is the effective incorporation of dopant ions (rather than merely decorating the surface) if the valence state or ionic radii of dopant and substituted ions are different.

Particles with sizes in the range of tens to hundreds of nm can be considered neither as quantum dots nor bulk material. They are not 'real' quantum systems, where quantum confinement plays an important role. Nevertheless, these particle sizes are interesting for incorporation in transparent, refractive index-matched matrices for reducing scattering losses. Drawbacks of these small particle sizes are a much larger surface to volume ratio, leading to stronger influence of non-radiative decay paths caused by surface defects. This can negatively affect the quantum efficiency and the thermal quenching behavior. Also dopant incorporation can be less straightforward for smaller particles.

6. Conclusions and perspectives.

The attractiveness of LEDs, stemming from their high efficiency in combination with a long lifetime and compact design, positions them as the prime general lighting technology for the (near) future. Furthermore, the phosphor-based approach is currently preferred over the combination of three (or four) quasi-monochromatic LEDs, explaining the current world-wide research effort in phosphor development. Although many phosphor systems (i.e. suitable host-dopant combinations) have been proposed in the last decade, a relatively small number of phosphors are actually suited to fulfill all requirements to arrive at an efficient white LED, with perfect white color and good color rendering. To assess the latter aspect, we have given here an overview of different color rendering metrics,

focusing on the color rendering index (CRI) and the color quality scale (CQS). It is clear that a decent light source should show emission bands (or lines) spread out over the entire visible range to accurately render all colors.

In this paper we put forward six requirements for LED phosphor materials, based on which the following conclusions can be made:

1. For high color rendering applications, the broad band emitting phosphors, such as Eu^{2+}, Ce^{3+} and Mn^{2+} are most suited.
2. The excitation spectrum should have a large overlap with the pumping LED, which is (often) not the case for the rare earth 4f-4f line emitters and Mn^{2+}, unless suitable sensitizers are found.
3. For the elevated temperatures reached in the proximity of the LED chip, the emission spectrum and intensity of the phosphor should resemble those at room temperature, to allow a stable performance as function of driving current and ambient temperature. The influence of temperature on the phosphor's luminescence is not systematically reported in literature, although the thermal quenching behavior is of the utmost importance. Most phosphors fail on this criterion.
4. The quantum efficiency should be as high as possible, to maximize the overall electrical-to-optical conversion efficiency of the entire LED-phosphor package. Often, it is not reported, although its determination is relatively straightforward. Obviously, it is hard for any newly developed phosphors to match the 90% quantum efficiency of the YAG:Ce benchmark.
5. The stability of phosphor materials favors certain hosts over others (e.g. nitrides over sulfides), although reports on the chemical and photo-thermal stability of phosphors are relatively rare. Encapsulation techniques have proven to considerably enhance the stability.

6. In high flux devices, the conversion process should not show saturation. For Eu^{2+} and Ce^{3+} this is no issue, while for the slower decaying 4f-4f rare earth ions and Mn^{2+} this can be a problem.

A good phosphor should fulfill all six requirements simultaneously, and hence reports on new phosphors for light-emitting diodes should discuss all six. Only then a true evaluation of its usefulness is possible. Especially measurements of the thermal behavior and the quantum efficiency are often lacking, although they are primordial in the evaluation. Nevertheless, the current impetus in phosphor research leads to the development of myriads of new phosphors, along with the rediscovery and optimization of 'forgotten' phosphors which were studied with different applications in mind. Although many phosphors fail on one or more aspects, many dopant-host combinations are promising and deserve further in-depth research. Also, phosphor development is still largely based on trial-and-error in selecting suitable hosts and (co)dopants. A firm theoretical background and modeling of the factors affecting the luminescence properties is therefore desirable as well.

In section 5.2.1. we discussed YAG:Ce^{3+} against the six requirements. It turned out that this phosphor does very well on all of them, especially if one can keep the dopant concentration low, e.g. by using translucent YAG:Ce ceramic plates, so that the thermal quenching is almost unnoticeable. However, for lighting devices with low color temperature or high color rendering, the most simple device architecture, i.e. a blue LED with a single (YAG:Ce^{3+}) phosphor is not sufficient. We can now answer the question which phosphors are fulfilling all requirements or summarize in what direction one should look. When taking the parameters of good excitability in the near-UV to blue part of the spectrum and a short decay time into account, along with the possibility to tune the emission spectrum, the rare earth ions Eu^{2+} and Ce^{3+} are clearly the best options. Then it comes down to choosing the appropriate host, as it will not only determine the excitation and emission spectra of these ions, but also the thermal quenching behavior and the (chemical and photo-thermal) stability. For the phosphors emitting in the red part of the spectrum, oxynitrides and nitrides are clearly the

hosts of choice. This is an entirely new class of luminescent materials, and its exploration is still underway. As shown in Table 2, several decent (oxy)nitride phosphors are already available, when taking the quantum efficiency and the thermal quenching into account.

Even if a phosphor gets high marks on all six requirements, the actual device development (phosphors in combination with pumping LEDs) involves several other considerations, such as the ease and the environmental friendliness of the synthesis method and ultimately also the cost of the material. Physical properties of phosphors (such as the particle size) can influence the overall device efficiency (e.g. through scattering losses). Two or more phosphors are in general required for high color rendering applications, where reabsorption negatively affects the efficiency. Therefore the development of red phosphors, preferably with a relatively narrow emission band, characterized by a large Stokes' shift would be favorable.

The future is bright for LEDs. Their unsurpassed efficiency and compactness makes them the prime illumination source of the future, allowing strong power reductions and new luminaire designs. LED's turn on the light [161]!

Acknowledgments

The authors wish to thank Wendy Davis from NIST for providing the NIST-CQS software. Part of this work was conducted in the framework of the interdisciplinary research platform NB-Photonics at Ghent University, Belgium.

Table caption:

Table 2. Key parameters for a selection of LED phosphors: peak emission wavelength (λ_{em}), quenching temperature $T_{0.5}$ (temperature for which the integrated emission intensity is half of that at low temperature), emission intensity at the specified temperature compared to room temperature (I/I_{RT}), internal and external quantum efficiencies (QE).

Figure captions:

Fig. 1. The history of the luminous efficacy in incandescent, halogen, fluorescent and sodium-vapor lamps and white LEDs. Adapted from [2]. Copyright IOP publishing. Reproduced with permission.

Fig. 2. Normalized spectral eye sensitivity curves for photopic vision V (λ) (full line) and scotopic vision V'(λ) (dashed line), as specified by the CIE.

Fig. 3. (a) 5mm, 20mA white LED, **(b)** schematic structure of the LED's cross-section along the plane perpendicular to the image (a) and indicated by the white arrows, **(c)** elemental mapping of selected elements using EDX (energy-dispersive x-ray analysis), with the maps for Y, Al and Ga indicating the $Y_3Al_5O_{12}$:Ce phosphor powder, the sapphire substrate and the (Ga,In)N diode, respectively. Adapted from [129]. **(d)** Schematic structure of a high-power package. Note the improved thermal management and the presence of an electrostatic discharge (ESD) protection. Adapted from [130], reproduced with permission.

Fig. 4. CQS **(left)** and LER **(center)** for a white light source with CCT of 3000K consisting of two variable emission bands (FWHM of 10nm) and one emission band fixed at 460nm (FWHM of 10nm). On the center image, the contour line for CQS equal to 70 is superposed in white. **Right:** The emission spectrum indicated by the black dot in the center image.

Fig. 5. CQS **(left)** and LER **(center)** for a white light source with CCT of 4500K consisting of two variable emission bands (FWHM of 10nm) and one emission band fixed at 460nm (FWHM of 10nm).

On the center image, the contour line for CQS equal to 70 is superposed in white. **Right:** The emission spectrum indicated by the black dot in the center image.

Fig. 6. CQS **(left)** and LER **(center)** for a white light source with CCT of 3000K consisting of two variable emission bands (FWHM of 50nm (G) and 70nm(R)) and one emission band fixed at 460nm (FWHM of 30nm). On the center image, the contour lines for CQS equal to 85 and 90 are superposed in white. **Right:** The emission spectrum indicated by the black dot in the center image.

Fig. 7. CQS **(left)** and LER **(center)** for a white light source with CCT of 4500K consisting of two variable emission bands (FWHM of 50nm (G) and 70nm(R)) and one emission band fixed at 460nm (FWHM of 30nm). On the center image, the contour lines for CQS equal to 85 and 90 are superposed in white. **Right:** The emission spectrum indicated by the black dot in the center image.

Fig. 8. Temperature dependence of the integrated emission intensity and luminescence decay times for $SrSi_2O_2N_2:Eu^{2+}$[2%]. Adapted from [50], Copyright 2009 American Chemical.

Fig. 9. Accelerated aging at 80% relative humidity and 80°C of (A) uncoated $CaS:Eu^{2+}$ particles and (B) coated with sol-gel prepared Al_2O_3. Photoluminescence intensity was measured in situ upon excitation with a 440nm LED [60]. Copyright (2010), with permission from Elsevier.

Fig. 10. Normalized emission spectra for a white LED as function of the driving current. The white LED is composed of a UV pumping LED, blue and green Eu^{2+} phosphors and red Eu^{2+}-Mn^{2+} phosphor. Adapted from [64], reproduced by permission of The Electrochemical Society.

Fig. 11. Energy level diagram for the free (gaseous) Ce^{3+} ion and for $Y_3Al_5O_{12}:Ce^{3+}$, where the effects of the centroid shift and the crystal field on the degenerate 5d level are indicated. For the ^2D levels of the free ion, the average energy is indicated. The position of the $^5d_4$ level is uncertain [162]. On the right a simplified configurational coordinate diagram (c.c.) is shown.

Fig. 12. Diffuse reflection spectra for $Sr_{2-x}Eu_xSi_5N_8$. Adapted from **[77]**, copyright (2006), with permission from Elsevier.

Fig. 13. Emission and excitation spectra for $Y_3Al_5O_{12}$:Ce[0.033%] and $Y_3Al_5O_{12}$:Ce[3.3%]. Adapted from [45], copyright 2009 American Chemical Society.

Fig. 14. (a) Excitation spectrum for the red Eu^{3+} emission in Y_2O_2S. Adapted from [163], copyright (2008), with permission from Elsevier. **(b)** Excitation (λ_{em} = 594nm) and **(c)** emission (λ_{exc} = 395nm) spectra for orange-emitting $Ba_{1.9}Eu_{0.05}Li_{0.05}CaMoO_6$. Adapted from [102], reproduced by permission of The Electrochemical Society.

Fig. 15. Emission wavelength of Eu^{2+}-doped compounds, adapted from [87]. Data (in red) are shown for recently reported Eu^{2+}-doped **(a)** oxynitride and **(b)** nitride phosphors. Copyright (2003), with permission from Elsevier.

Fig. 16. (Bottom) Schematic view of a white LED with a Lumiramic (YAG:Ce) phosphor plate on top of the pumping LED. (Top) Color deviation for LUXEON LEDs (Philips) from the intended device color for >150k phosphor-based LEDs (blue) and when using ceramic phosphor plates (red). Adapted from [164], reproduced with permission.

Fig. 17. (left) Dependency on drive current of a 2-pc-LED emission, using two (oxy)nitride phosphors, up to 4A (2W/mm² optical pump power) and **(right)** CCT and R_a with drive current and temperature (shown for 25 and 125 °C). Adapted from [40], Copyright Wiley-VCH Verlag GmbH & Co. KGaA. Reproduced with permission.

Fig. 18. Three-band white LED combining a blue InGaN chip, green-emitting CdSe-ZnSe QDs and red-emitting CdSe-ZnSe QDs. Adapted from [165], (© 2006 IEEE) Reproduced with permission.

1. N. Zheludev, *Nature Photonics*, **1**, 189 (2007).

2. Y. Narukawa, M. Ichikawa, D. Sanga, M. Sano and T. Mukai, *J. Phys. D-Appl. Phys.*, **43**, 354002 (2010).

3. E. F. Schubert, J. K. Kim, H. Luo and J. Q. Xi, *Reports on Progress in Physics*, **69**, 3069 (2006).

4. J. M. Phillips, M. E. Coltrin, M. H. Crawford, A. J. Fischer, M. R. Krames, R. Mueller-Mach, G. O. Mueller, Y. Ohno, L. E. S. Rohwer, J. A. Simmons and J. Y. Tsao, *Laser & Photonics Reviews*, **1**, 307 (2007).

5. J. E. Van Haecke, P. F. Smet and D. Poelman, *Spectrochimica Acta Part B-Atomic Spectroscopy*, **59**, 1759 (2004).

6. D. Poelman, N. Avci and P. F. Smet, *Optics Express*, **17**, 358 (2009).

7. M. S. Rea, J. D. Bullough, J. P. Freyssinier-Nova and A. Bierman, *Lighting Research and Technology*, **36**, 85 (2004).

8. W. Kondro, *Canadian Medical Association Journal*, **177**, 136 (2007).

9. P. Autier, *European Journal of Cancer*, **40**, 2367 (2004).

10. A. F. McKinlay, J. H. Bernhardt, A. Ahlbom, J. P. Cesarini, F. R. de Gruijl, M. Hietanen, R. Owen, D. H. Sliney, P. Soderberg, A. J. Swerdlow, M. Taki, T. S. Tenforde, P. Vecchia, B. Veyret, R. Matthes, M. H. Repacholi, B. Diffey, M. A. Mainster, T. Okuno and B. E. Stuck, *Health Physics*, **87**, 171 (2004).

11. S. L. McColl and J. A. Veitch, *Psychological Medicine*, **31**, 949 (2001).

12. M. Khazova and J. B. O'Hagan, *Radiation Protection Dosimetry*, **131**, 521 (2008).

13. Directive 2006/25/EC of the European Parliament and of the Council, *Official Journal of the European Union*, L114/38-59/EN (2006).

14. CREE, LED eye safety application note CLD-AP34, Cree Inc., Durham, NC (2009).

15. T. Kozaki, S. Koga, N. Toda, H. Noguchi and A. Yasukouchi, *Neuroscience Letters*, **439**, 256 (2008).

16. M. Rea, M. Figueiro, A. Bierman and J. Bullough, *Journal of Circadian Rhythms*, **8**, 2 (2010).

17. S. Lehrl, K. Gerstmeyer, J. H. Jacob, H. Frieling, A. W. Henkel, R. Meyrer, J. Wiltfang, J. Kornhuber and S. Bleich, *Journal of Neural Transmission*, **114**, 457 (2007).

18. M. Kondo, D. Kanikowska and H. Tokura, *Collegium Antropologicum*, **31**, 969 (2007).

19. CIE, Method of measuring and specifying colour rendering properties of light sources, *CIE Technical Report*, **13**, E-1.3.2 (1965).

20. CIE, Method of measuring and specifying color-rendering properties of light sources, *CIE Publication*, TC-3.2 (1974).

21. CIE, Method of measuring and specifying colour rendering properties of light source, *CIE Technical Report* 13.3:1995 (1995).

22. J. E. Schanda, *Colorimetry: understanding the CIE system*, Wiley, Hoboken, New Jersey (2007).

23. CIE, in *Proc. of the 16th session of the CIE*, **A**, p. 95, Washington (1967).

24. P. Bodrogi, P. Csuti, F. Szabó and J. Schanda, in *Proc. CIE Expert Symp. LED Light Sources: Phys. Meas. Visual Photobiol. Assess.* , p. 24, Tokyo (2004).

25. W. Davis and Y. Ohno, in *SPIE Fifth International Conference on Solid State Lighting*, **5941**, p. 59411G (2005).

26. W. Davis and Y. Ohno, *Opt. Eng.*, **49**, 16 (2010).

27. D. B. Judd, *Illum. Eng.*, **62**, 593 (1967).

28. W. A. Thornton, *Journal of the Optical Society of America*, **61**, 1155 (1971).

29. X. Guo and K. W. Houser, *Lighting Research and Technology*, **36**, 183 (2004).

30. K. Hashimoto, T. Yano, M. Shimizu and Y. Nayatani, *Color Research and Application*, **32**, 361 (2007).

31. F. Szabó, P. Bodrogi and J. Schanda, *Lighting Research and Technology*, **41**, 165 (2009).

32. C. Hoelen, J. Ansems, P. Deurenberg, T. Treurniet, E. van Lier, O. Chao, V. Mercier, G. Calon, K. van Os, G. Lijten and J. Sondag-Huethorst, in *Fifth International Conference on Solid State Lighting*, **5941**, p. 59410A, San Diego, CA, USA (2005).

33. Y. Gu, N. Narendran, T. Dong and H. Wu, in *Sixth International Conference on Solid State Lighting*, **6337**, p. 63370J, San Diego, CA, USA (2006).

34. M. R. Krames, O. B. Shchekin, R. Mueller-Mach, G. O. Mueller, Z. Ling, G. Harbers and M. G. Craford, *Journal of Display Technology*, **3**, 160 (2007).

35. Y. Hu, W. Zhuang, H. Ye, S. Zhang, Y. Fang and X. Huang, *Journal of Luminescence*, **111**, 139 (2005).

36. T. Horikawa and et al., *IOP Conference Series: Materials Science and Engineering*, **1**, 012024 (2009).

37. R. Mueller-Mach, G. O. Mueller, M. R. Krames and T. Trottier, *Ieee Journal of Selected Topics in Quantum Electronics*, **8**, 339 (2002).

38. H. Wu, X. M. Zhang, C. F. Guo, R. Xu, M. M. Wu and Q. Su, *IEEE Photonics Technol. Lett.*, **17**, 1160 (2005).

39. Y. Shimomura, T. Honma, M. Shigeiwa, T. Akai, K. Okamoto and N. Kijima, *Journal of the Electrochemical Society*, **154**, J35 (2007).

40. R. Mueller-Mach, G. Mueller, M. R. Krames, H. A. Hoppe, F. Stadler, W. Schnick, T. Juestel and P. Schmidt, *Physica Status Solidi a-Applications and Materials Science*, **202**, 1727 (2005).

41. C. C. Yang, C. M. Lin, Y. J. Chen, Y. T. Wu, S. R. Chuang, R. S. Liu and S. F. Hu, *Applied Physics Letters*, **90**, 123503 (2007).

42. A. A. Setlur, E. V. Radkov, C. S. Henderson, J. H. Her, A. M. Srivastava, N. Karkada, M. S. Kishore, N. P. Kumar, D. Aesram, A. Deshpande, B. Kolodin, L. S. Grigorov and U. Happek, *Chem. Mat.*, **22**, 4076 (2010).

43. N. Kimura, K. Sakuma, S. Hirafune, K. Asano, N. Hirosaki and R. J. Xie, *Applied Physics Letters*, **90**, 051109 (2007).

44. C. H. Huang and T. M. Chen, *Optics Express*, **18**, 5089 (2010).

45. V. Bachmann, C. Ronda and A. Meijerink, *Chem. Mat.*, **21**, 2077 (2009).

46. R. Mueller-Mach, G. O. Mueller, M. R. Krames, O. B. Shchekin, P. J. Schmidt, H. Bechtel, C. H. Chen and O. Steigelmann, *physica status solidi (RRL) – Rapid Research Letters*, **3**, 215 (2009).

47. R. J. Xie, N. Hirosaki, N. Kimura, K. Sakuma and M. Mitomo, *Applied Physics Letters*, **90**, 191101 (2007).

48. R. J. Xie, N. Hirosaki and T. Takeda, *Appl. Phys. Express*, **2**, 022401 (2009).

49. Y. Umetsu, S. Okamoto and H. Yamamoto, *Journal of the Electrochemical Society*, **155**, J193 (2008).

50. V. Bachmann, C. Ronda, O. Oeckler, W. Schnick and A. Meijerink, *Chem. Mat.*, **21**, 316 (2009).

51. P. Dorenbos, *Journal of Physics-Condensed Matter*, **17**, 8103 (2005).

52. P. Dorenbos and E. van der Kolk, *Opt. Mater.*, **30**, 1052 (2008).

53. A. L. Heyes, *Journal of Luminescence*, **129**, 2004 (2009).

54. M. M. Haque, H. I. Lee and D. K. Kim, *Journal of Alloys and Compounds*, **481**, 792 (2009).

55. R.-J. Xie, N. Hirosaki, Y. Li and T. Takeda, *Materials*, **3**, 3777 (2010).

56. N. Narendran, Y. Gu, J. P. Freyssinier, H. Yu and L. Deng, *Journal of Crystal Growth*, **268**, 449 (2004).

57. H. H. Shin, J. H. Kim, B. Y. Han and J. S. Yoo, *Japanese Journal of Applied Physics*, **47**, 3524 (2008).

58. N. Avci, J. Musschoot, P. F. Smet, K. Korthout, A. Avci, C. Detavernier and D. Poelman, *Journal of the Electrochemical Society*, **156**, J333 (2009).
59. S. H. Yoo and C. K. Kim, *Journal of the Electrochemical Society*, **156**, J170 (2009).
60. N. Avci, I. Cimieri, P. F. Smet and D. Poelman, *Opt. Mater.*, **In Press, DOI: 10.1016/j.optmat.2010.07.021** (2010).
61. A. A. Setlur, J. J. Shiang and U. Happek, *Applied Physics Letters*, **92**, 081104 (2008).
62. K. Park, N. Choi, J. Kim, P. Kung and S. M. Kim, *Solid State Communications*, **150**, 329 (2010).
63. U. Happek, A. A. Setlur and J. J. Shiang, *Journal of Luminescence*, **129**, 1459 (2009).
64. T. G. Kim, Y. S. Kim and S. J. Im, *Journal of the Electrochemical Society*, **156**, J203 (2009).
65. S. H. M. Poort, A. Meyerink and G. Blasse, *Journal of Physics and Chemistry of Solids*, **58**, 1451 (1997).
66. P. Dorenbos, *Nuclear Instruments & Methods in Physics Research Section a-Accelerators Spectrometers Detectors and Associated Equipment*, **486**, 208 (2002).
67. W. M. Yen, S. Shionoya and H. Yamamoto, *Phosphor Handbook, second edition*, CRC Press, Boca Raton, FL, USA (2007).
68. Q. Xia, M. Batentschuk, A. Osvet, A. Winnacker and J. Schneider, *Radiation Measurements*, **45**, 350 (2010).
69. P. F. Smet, N. Avci, B. Loos, J. E. Van Haecke and D. Poelman, *Journal of Physics-Condensed Matter*, **19**, 246223 (2007).
70. P. F. Smet, N. Avci and D. Poelman, *Journal of the Electrochemical Society*, **156**, H243 (2009).
71. C. Chartier, C. Barthou, P. Benalloul and J. M. Frigerio, *Journal of Luminescence*, **111**, 147 (2005).
72. Y. R. Do, J. W. Bae, Y. Kim and H. G. Yang, *Bulletin of the Korean Chemical Society*, **21**, 295 (2000).
73. J. K. Park, C. H. Kim, S. H. Park, H. D. Park and S. Y. Choi, *Applied Physics Letters*, **84**, 1647 (2004).
74. K. B. Kim, Y. I. Kim, H. G. Chun, T. Y. Cho, J. S. Jung and J. G. Kang, *Chem. Mat.*, **14**, 5045 (2002).
75. L. H. Liu, R. J. Xie, N. Hirosaki, Y. Q. Li, T. Takeda, C. N. Zhang, J. G. Li and X. D. Sun, *Journal of the American Ceramic Society*, **93**, 2018 (2010).

76. W. Bin Im, S. Brinkley, J. Hu, A. Mikhailovsky, S. P. DenBaars and R. Seshadri, *Chem. Mat.*, **22**, 2842 (2010).

77. Y. Q. Li, J. E. J. van Steen, J. W. H. van Krevel, G. Botty, A. C. A. Delsing, F. J. DiSalvo, G. de With and H. T. Hintzen, *Journal of Alloys and Compounds*, **417**, 273 (2006).

78. R. J. Xie, N. Hirosaki, K. Sakuma and N. Kimura, *J. Phys. D-Appl. Phys.*, **41**, 144013 (2008).

79. H. L. Li, R. J. Xie, N. Hirosaki, T. Takeda and G. H. Zhou, *Int. J. Appl. Ceram. Technol.*, **6**, 459 (2009).

80. T. Kurushima, G. Gundiah, Y. Shimomura, M. Mikami, N. Kijima and A. K. Cheetham, *Journal of the Electrochemical Society*, **157**, J64 (2010).

81. H. Watanabe and N. Kijima, *Journal of Alloys and Compounds*, **475**, 434 (2009).

82. Y. Q. Li, N. Hirosaki, R. J. Xie, T. Takeda and M. Mitomo, *Chem. Mat.*, **20**, 6704 (2008).

83. E. Zych, C. Brecher, A. J. Wojtowicz and H. Lingertat, *Journal of Luminescence*, **75**, 193 (1997).

84. M. Mikami, S. Shimooka, K. Uheda, H. Imura and N. Kijima, in *Siaions and Non-Oxides*, K. Komeya, Y. B. Cheng, J. Tatami and M. Mitomo Editors, p. 11, Trans Tech Publications Ltd, Stafa-Zurich (2009).

85. H. L. Li, R. J. Xie, N. Hirosaki, T. Suehiro and Y. Yajima, *Journal of the Electrochemical Society*, **155**, J175 (2008).

86. R. J. Xie, N. Hirosaki, M. Mitomo, K. Takahashi and K. Sakuma, *Applied Physics Letters*, **88**, 101104 (2006).

87. P. Dorenbos, *Journal of Luminescence*, **104**, 239 (2003).

88. B. Dierre, X. L. Yuan, K. Inoue, N. Hirosaki, R. J. Xie and T. Sekiguchi, *Journal of the American Ceramic Society*, **92**, 1272 (2009).

89. K. Uheda, H. Takizawa, T. Endo, H. Yamane, M. Shimada, C. M. Wang and M. Mitomo, *Journal of Luminescence*, **87-9**, 967 (2000).

90. J. E. Van Haecke, P. F. Smet and D. Poelman, *Journal of the Electrochemical Society*, **152**, H225 (2005).

91. J. E. Van Haecke, P. F. Smet and D. Poelman, *Journal of Luminescence*, **126**, 508 (2007).

92. P. Dorenbos, *Journal of Physics-Condensed Matter*, **15**, 4797 (2003).

93. P. Dorenbos, *Journal of Luminescence*, **99**, 283 (2002).

94. Y. X. Pan, M. M. Wu and Q. Su, *Journal of Physics and Chemistry of Solids*, **65**, 845 (2004).
95. Y. Q. Li, G. de With and H. T. Hintzen, *Journal of Luminescence*, **116**, 107 (2006).
96. P. Dorenbos, *Journal of Physics-Condensed Matter*, **15**, 575 (2003).
97. P. Dorenbos, *Journal of Physics-Condensed Matter*, **15**, 2645 (2003).
98. S. Lizzo, A. Meijerink and G. Blasse, *Journal of Luminescence*, **59**, 185 (1994).
99. A. M. Srivastava and P. Dorenbos, *Journal of Luminescence*, **129**, 634 (2009).
100. V. Bachmann, T. Justel, A. Meijerink, C. Ronda and P. J. Schmidt, *Journal of Luminescence*, **121**, 441 (2006).
101. V. Bachmann, A. Meijerink and C. Ronda, *Journal of Luminescence*, **129**, 1341 (2009).
102. V. Sivakumar and U. V. Varadaraju, *Electrochemical and Solid State Letters*, **9**, H35 (2006).
103. H. Y. Chung, C. H. Lu and C. H. Hsu, *Journal of the American Ceramic Society*, **93**, 1838 (2010).
104. H. Y. Jiao and Y. H. Wang, *Journal of the Electrochemical Society*, **156**, J117 (2009).
105. W. R. Liu, C. C. Lin, Y. C. Chiu, Y. T. Yeh, S. M. Jang and R. S. Liu, *Optics Express*, **18**, 2946 (2010).
106. E. C. Fuchs, C. Sommer, F. P. Wenzl, B. Bitschnau, A. H. Paulitsch, A. Muhlanger and K. Gatterer, *Mater. Sci. Eng. B-Adv. Funct. Solid-State Mater.*, **156**, 73 (2009).
107. H. Lin, X. Y. Wang, C. M. Li, X. J. Li, S. Tanabe and J. Y. Yu, *Spectroc. Acta Pt. A-Molec. Biomolec. Spectr.*, **67**, 1417 (2007).
108. S. Okamoto and H. Yamamoto, *Electrochemical and Solid State Letters*, **10**, J139 (2007).
109. P. C. De Sousa and O. A. Serra, *Journal of Luminescence*, **129**, 1664 (2009).
110. B. Han, K. C. Mishra, M. Raukas, K. Klinedinst, J. Tao and J. B. Talbot, *Journal of the Electrochemical Society*, **154**, J262 (2007).
111. P. Boutinaud, E. Pinel, M. Oubaha, R. Mahiou, E. Cavalli and M. Bettinelli, *Opt. Mater.*, **28**, 9 (2006).
112. H. S. Jang, W. Bin Im, D. C. Lee, D. Y. Jeon and S. S. Kim, *Journal of Luminescence*, **126**, 371 (2007).
113. G. Blasse and B. C. Grabmaier, *Luminescent Materials*, Springer, Berlin, Germany (1994).
114. C. J. Duan, A. C. A. Delsing and H. T. Hintzen, *Chem. Mat.*, **21**, 1010 (2009).

115. C. J. Duan, W. M. Otten, A. C. A. Delsing and H. T. Hintzen, *Journal of Solid State Chemistry*, **181**, 751 (2008).

116. J. S. Kim, P. E. Jeon, Y. H. Park, J. C. Choi and H. L. Park, *Journal of the Electrochemical Society*, **152**, H29 (2005).

117. P. Yang, G. Q. Yao and J. H. Lin, *Opt. Mater.*, **26**, 327 (2004).

118. W. J. Xie, J. Y. Tang, L. Y. Hao and X. Xu, *Opt. Mater.*, **32**, 274 (2009).

119. G. Blasse, *Chemical Physics Letters*, **104**, 160 (1984).

120. P. L. Li, Z. J. Wang, Z. P. Yang and Q. L. Guo, *Journal of the Electrochemical Society*, **157**, H504 (2010).

121. J. S. Kim, P. E. Jeon, Y. H. Park, J. C. Choi, H. L. Park, G. C. Kim and T. W. Kim, *Applied Physics Letters*, **85**, 3696 (2004).

122. J. S. Kim, A. K. Kwon, Y. H. Park, J. C. Choi, H. L. Park and G. C. Kim, *Journal of Luminescence*, **122**, 583 (2007).

123. W. D. Wang, J. K. Tang, S. T. Hsu, J. Wang and B. P. Sullivan, *Chemical Physics Letters*, **457**, 103 (2008).

124. R. X. Zhong and J. H. Zhang, *Journal of Luminescence*, **130**, 206 (2010).

125. M. Y. Peng, N. Da, S. Krolikowski, A. Stiegelschmitt and L. Wondraczek, *Optics Express*, **17**, 21169 (2009).

126. M. Y. Peng and L. Wondraczek, *Journal of the American Ceramic Society*, **93**, 1437 (2010).

127. P. Dorenbos, *Journal of Luminescence*, **108**, 301 (2004).

128. S. Ye, F. Xiao, Y. X. Pan, Y. Y. Ma and Q. Y. Zhang, *Materials Science and Engineering: R: Reports*, **71**, 1 (2010).

129. P. F. Smet, I. Moreels, Z. Hens and D. Poelman, *Materials*, **3**, 2834 (2010).

130. E. F. Schubert, *Light-emitting diodes*, Cambridge University Press, Cambridge, UK (2006).

131. S. Nakamura, M. Senoh, N. Iwasa, S. Nagahama, T. Yamada and T. Mukai, *Japanese Journal of Applied Physics Part 2-Letters*, **34**, L1332 (1995).

132. G. Blasse and A. Bril, *Applied Physics Letters*, **11**, 53 (1967).

133. D. D. Jia, Y. Wang, X. Guo, K. Li, Y. K. Zou and W. Y. Jia, *Journal of the Electrochemical Society*, **154**, J1 (2007).

134. A. A. Setlur, *The Electrochemical Society Interface*, **18**, 32 (2009).

135. Y. S. Lin, R. S. Liu and B. M. Cheng, *Journal of the Electrochemical Society*, **152**, J41 (2005).

136. S. Fujita, A. Sakamoto and S. Tanabe, *Ieee Journal of Selected Topics in Quantum Electronics*, **14**, 1387 (2008).

137. R. Hansel, S. Allison and G. Walker, *Journal of Materials Science*, **45**, 146 (2010).

138. A. Katelnikovas, H. Bettentrup, D. Uhlich, S. Sakirzanovas, T. Justel and A. Kareiva, *Journal of Luminescence*, **129**, 1356 (2009).

139. A. Katelnikovas, T. Bareika, P. Vitta, T. Justel, H. Winkler, A. Kareiva, A. Zukauskas and G. Tamulaitis, *Opt. Mater.*, **32**, 1261 (2010).

140. H. Bechtel, P. Schmidt, W. Busselt and B. S. Schreinemacher, in *Proceedings of SPIE - The International Society for Optical Engineering*, **7058** (2008).

141. K. N. Kim, J. M. Kim, K. J. Choi, J. K. Park and C. H. Kim, *Journal of the American Ceramic Society*, **89**, 3413 (2006).

142. C. R. Wang, K. B. Tang, Q. Yang, C. H. An, B. Hai, G. Z. Shen and Y. T. Qian, *Chemical Physics Letters*, **351**, 385 (2002).

143. K. Korthout, P. F. Smet and D. Poelman, *Applied Physics Letters*, **94**, 051104 (2009).

144. P. F. Smet, K. Korthout, J. E. Van Haecke and D. Poelman, *Mater. Sci. Eng. B-Solid State Mater. Adv. Technol.*, **146**, 264 (2008).

145. T. W. Kuo, W. R. Liu and T. M. Chen, *Optics Express*, **18**, 8187 (2010).

146. K. S. Sohn, D. H. Park, S. H. Cho, J. S. Kwak and J. S. Kim, *Chem. Mat.*, **18**, 1768 (2006).

147. R. J. Xie and N. Hirosaki, *Sci. Technol. Adv. Mater.*, **8**, 588 (2007).

148. X. H. He, N. Lian, J. H. Sun and M. Y. Guan, *Journal of Materials Science*, **44**, 4763 (2009).

149. J. K. Park, M. A. Lim, C. H. Kim, H. D. Park, J. T. Park and S. Y. Choi, *Applied Physics Letters*, **82**, 683 (2003).

150. S. H. M. Poort, W. Janssen and G. Blasse, *Journal of Alloys and Compounds*, **260**, 93 (1997).

151. J. K. Park, K. J. Choi, J. H. Yeon, S. J. Lee and C. H. Kim, *Applied Physics Letters*, **88**, 043511 (2006).

152. H. S. Jang, H. Yang, S. W. Kim, J. Y. Han, S. G. Lee and D. Y. Jeon, *Adv. Mater.*, **20**, 2696 (2008).

153. J. S. Kim, Y. H. Park, S. M. Kim, J. C. Choi and H. L. Park, *Solid State Communications*, **133**, 445 (2005).

154. S. Neeraj, N. Kijima and A. K. Cheetham, *Chemical Physics Letters*, **387**, 2 (2004).

155. W. Chung, K. Park, H. J. Yu, J. Kim, B. H. Chun and S. H. Kim, *Opt. Mater.*, **32**, 515 (2010).

156. E. Jang, S. Jun, H. Jang, J. Llim, B. Kim and Y. Kim, *Adv. Mater.*, **22**, 3076 (2010).

157. C. J. Summers, H. M. Menkara, R. A. Gilstrap, M. Menkara and T. Morris, *Materials Science Forum*, **654-656**, 1130 (2010).

158. H. J. Byun, W. S. Song, Y. S. Kim and H. Yang, *J. Phys. D-Appl. Phys.*, **43**, 195401 (2010).

159. R. Schmechel, M. Kennedy, H. von Seggern, H. Winkler, M. Kolbe, R. A. Fischer, X. M. Li, A. Benker, M. Winterer and H. Hahn, *J. Appl. Phys.*, **89**, 1679 (2001).

160. H. S. Yang, S. Santra and P. H. Holloway, *Journal of Nanoscience and Nanotechnology*, **5**, 1364 (2005).

161. A. Meijerink, V. Bachmann and C. Ronda, LED's turn on the light, in *ESTE 2010*, Piechowice - Wroclaw (2010).

162. P. A. Tanner, L. S. Fu, L. X. Ning, B. M. Cheng and M. G. Brik, *Journal of Physics-Condensed Matter*, **19**, 216213 (2007).

163. C. F. Guo, L. Luan, C. H. Chen, D. X. Huang and Q. Su, *Materials Letters*, **62**, 600 (2008).

164. Philips, Press information, "New Luxeon Rebel leds set benchmarks for illumination application efficiency and quality of light", (2010).

165. H. S. Chen, C. K. Hsu and H. Y. Hong, *IEEE Photonics Technol. Lett.*, **18**, 193 (2006).

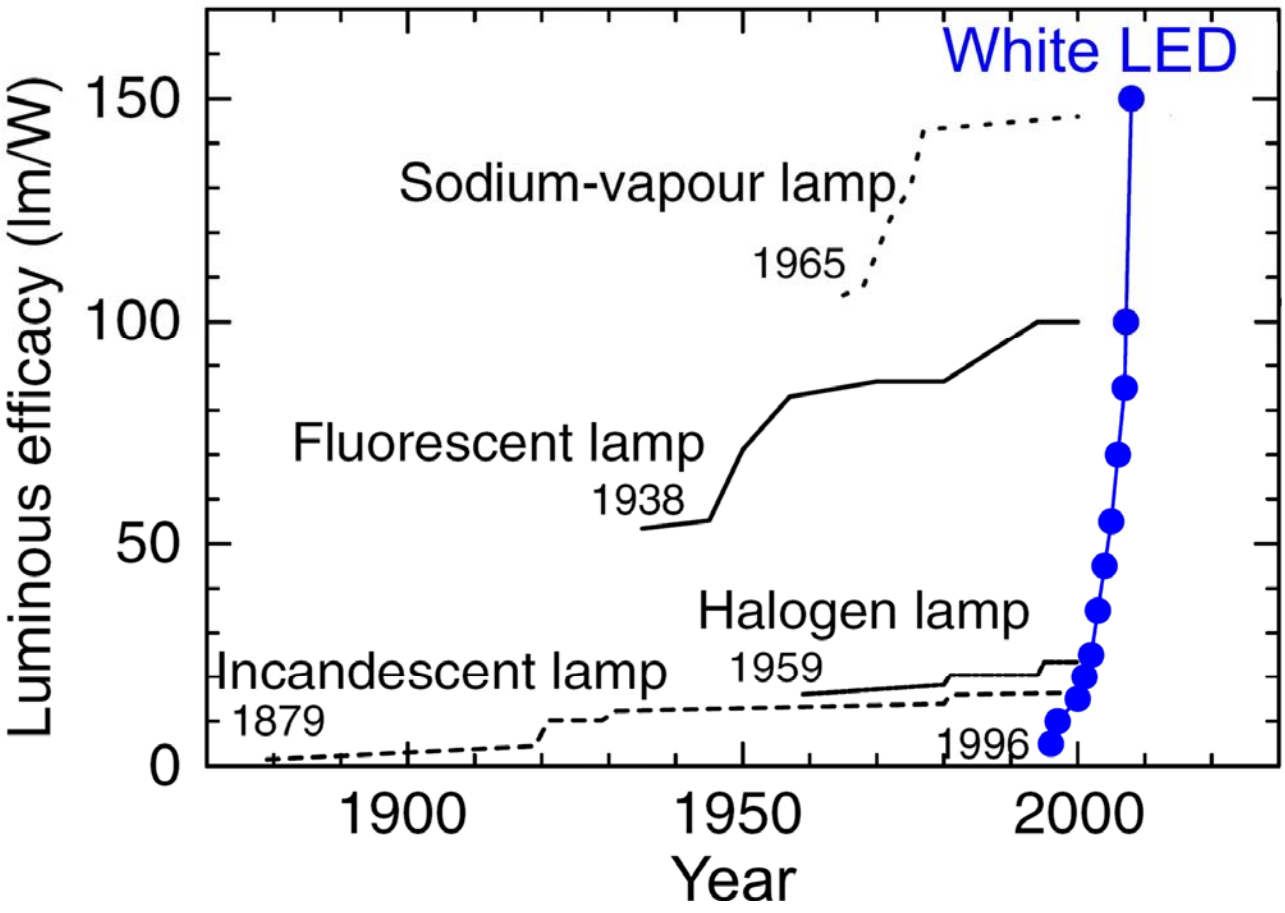
White LED
Sodium-vapour lamp
1965
Fluorescent lamp
1938
Halogen lamp
1959
Incandescent lamp
1879
1996
Luminous efficacy (lm/W)
150
100
50
0
1900
1950
2000
Year

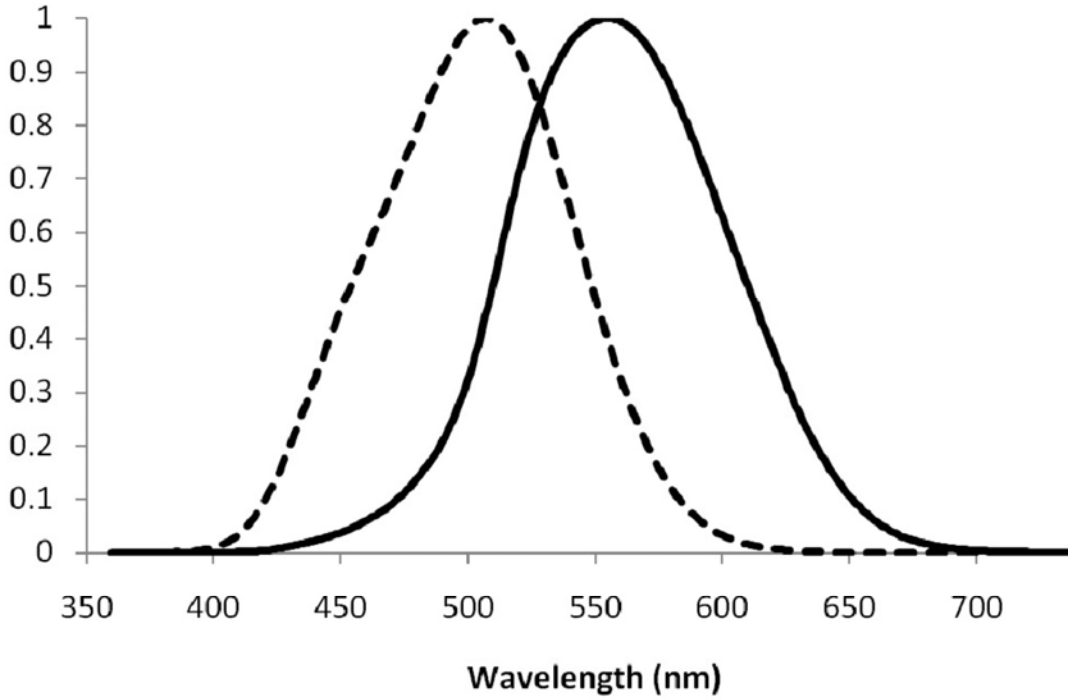
1
0.9
0.8
0.7
0.6
0.5
0.4
0.3
0.2
0.1
0
350
400
450
500
550
600
650
700
Wavelength (nm)

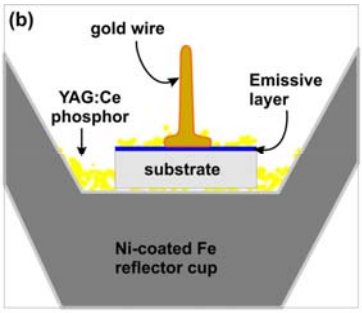
(b)
gold wire
YAG:Ce
phosphor
Emissive
layer
substrate
Ni-coated Fe
reflector cup


(a)

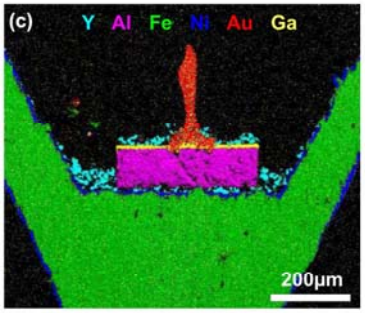
(c)
Y Al Fe Ni Au Ga
200µm

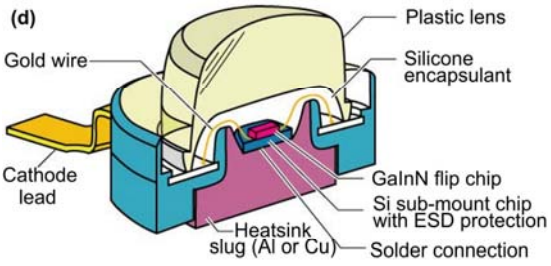
(d)
Plastic lens
Gold wire
Silicone
encapsulant
Cathode
lead
GaInN flip chip
Si sub-mount chip
with ESD protection
Heatsink
slug (Al or Cu)
Solder connection

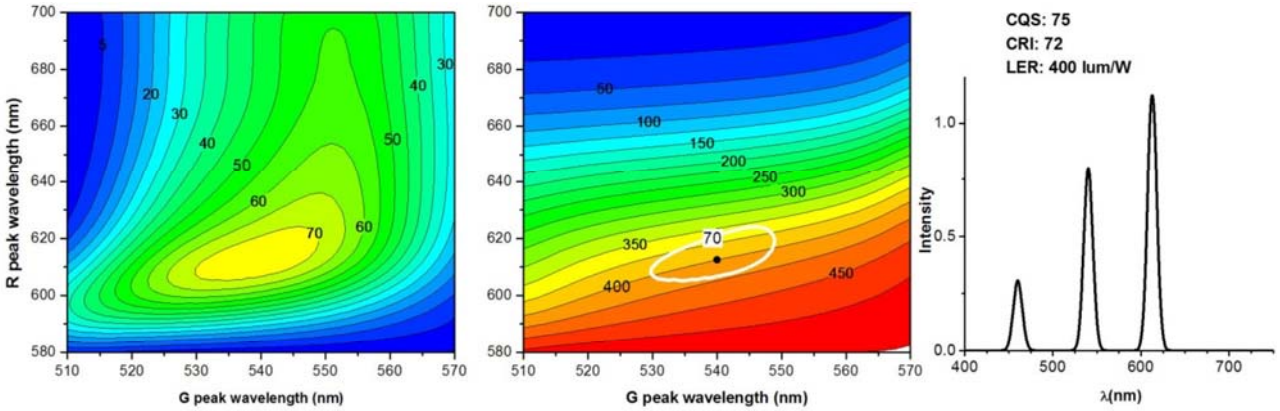
R peak wavelength (nm)
G peak wavelength (nm)
G peak wavelength (nm)
Intensity
λ(nm)
CQS: 75
CRI: 72
LER: 400 lum/W

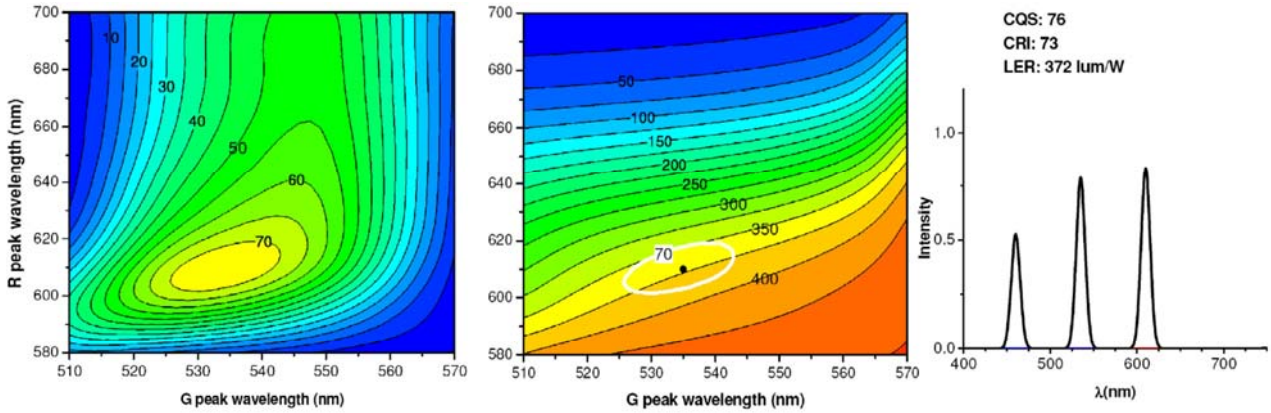
R peak wavelength (nm)
G peak wavelength (nm)
10
20
30
40
50
60
70
G peak wavelength (nm)
50
100
150
200
250
300
350
70
400
CQS: 76
CRI: 73
LER: 372 lum/W
Intensity
λ(nm)

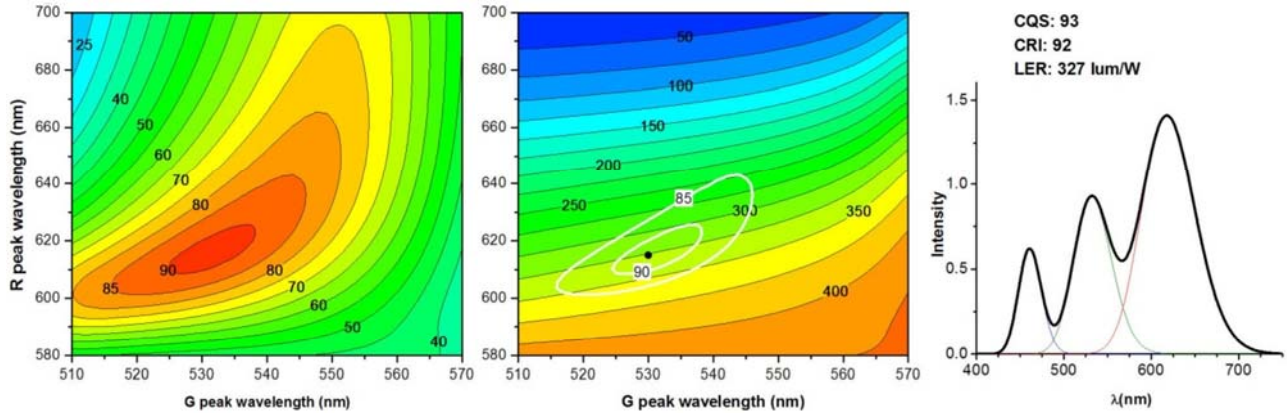
R peak wavelength (nm)
G peak wavelength (nm)
25
40
50
60
70
80
90
85
80
70
60
50
40
G peak wavelength (nm)
50
100
150
200
250
85
300
350
90
400
CQS: 93
CRI: 92
LER: 327 lum/W
Intensity
λ(nm)

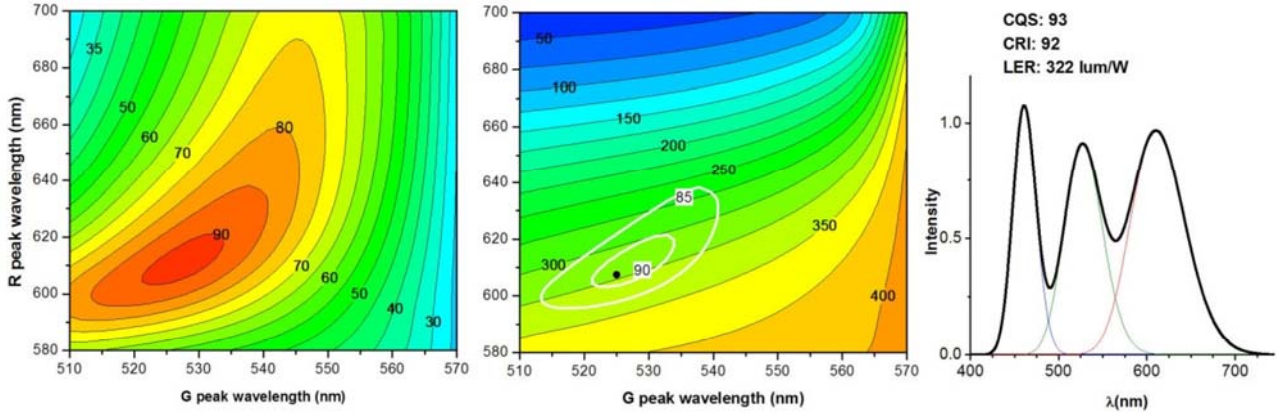
R peak wavelength (nm)
G peak wavelength (nm)
35
50
60
70
80
90
70
60
50
40
30
G peak wavelength (nm)
50
100
150
200
250
85
350
300
90
400
CQS: 93
CRI: 92
LER: 322 lum/W
Intensity
λ(nm)

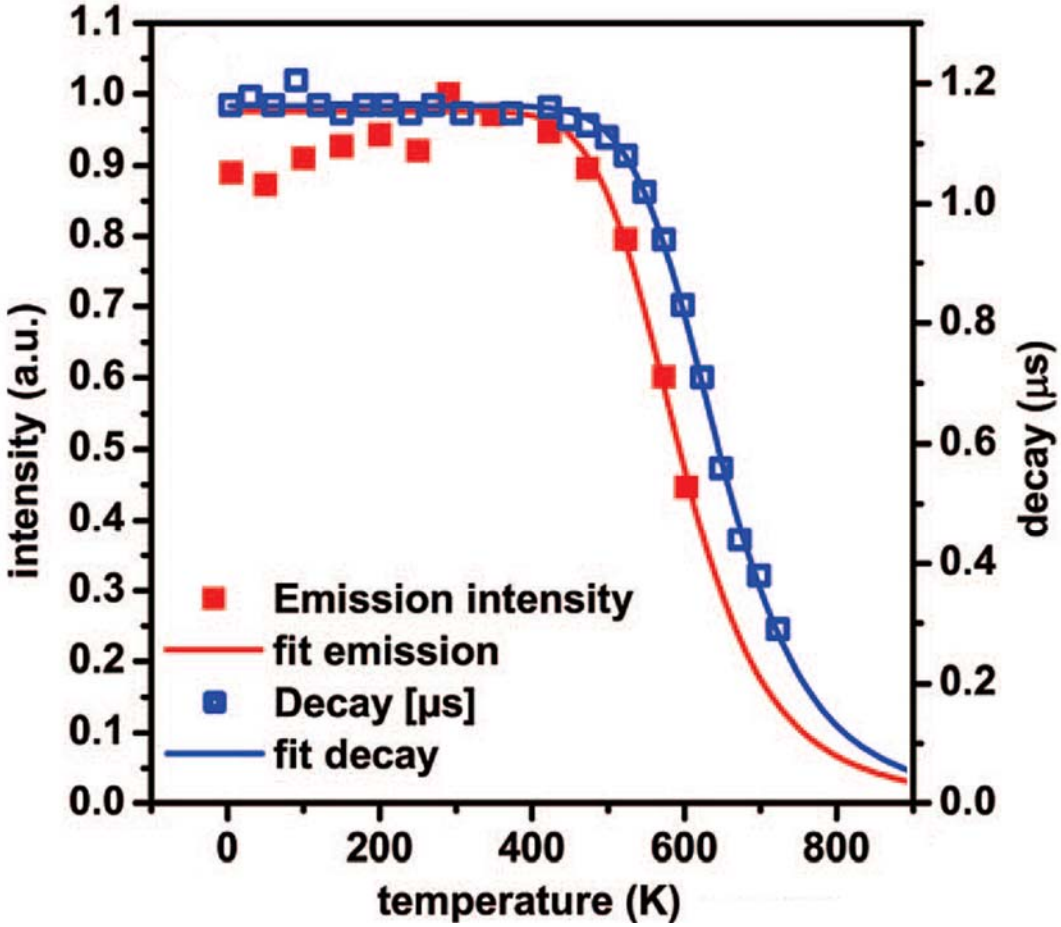
intensity (a.u.)
decay (µs)
temperature (K)
Emission intensity
fit emission
Decay [µs]
fit decay
0.0
0.1
0.2
0.3
0.4
0.5
0.6
0.7
0.8
0.9
1.0
1.1
1.2
0
200
400
600
800

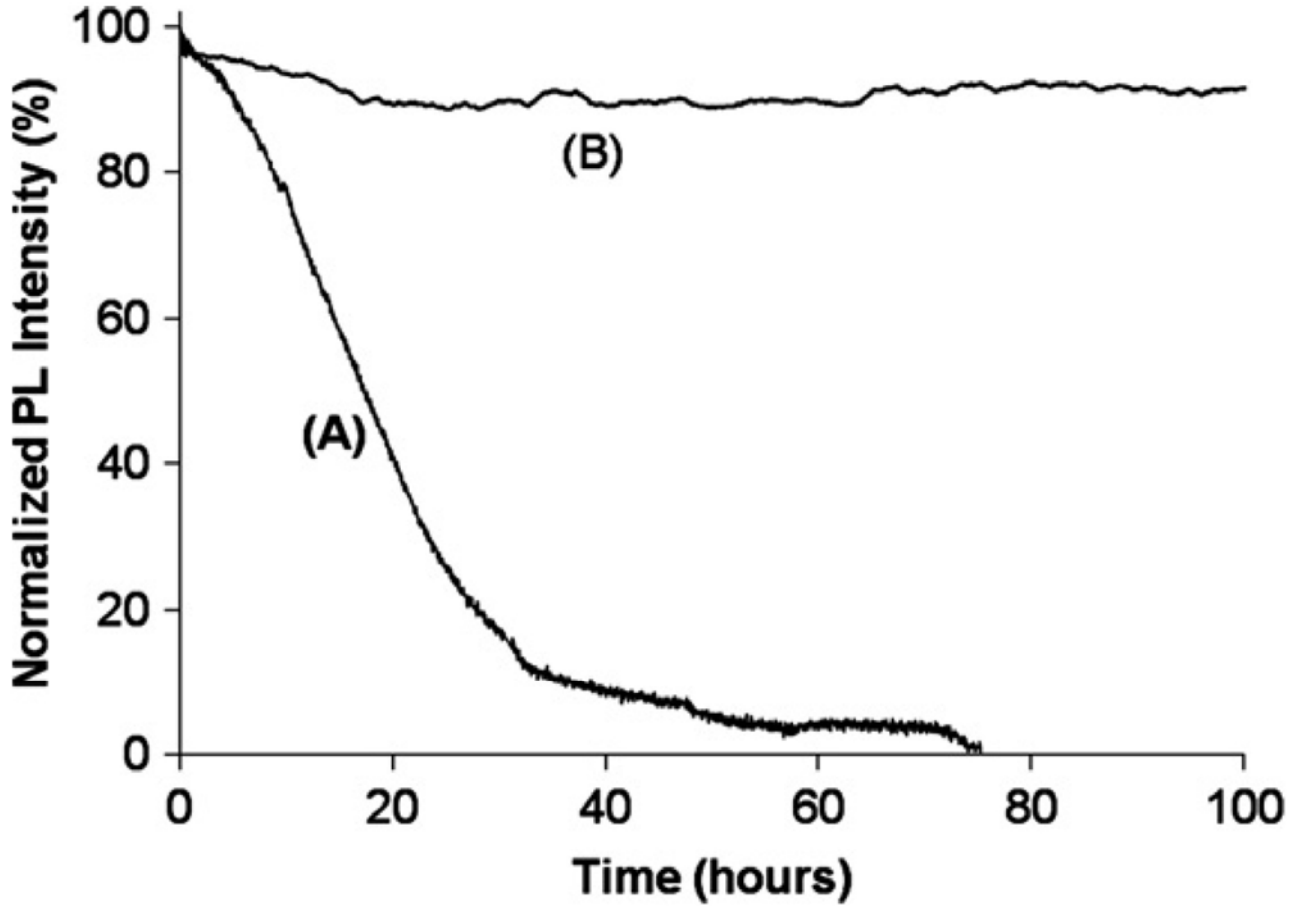
Normalized PL Intensity (%)
100
80
60
40
20
0
0
20
40
60
80
100
Time (hours)
(A)
(B)

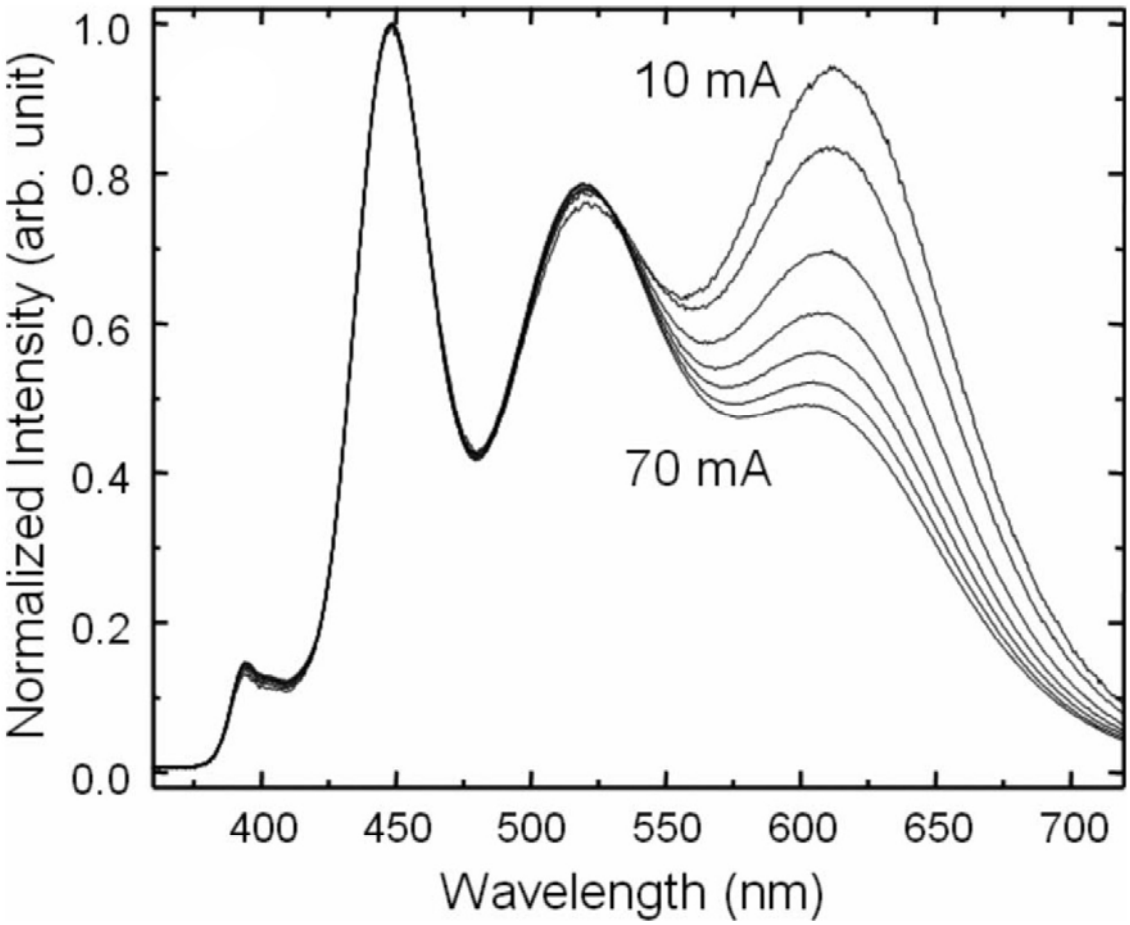
Normalized Intensity (arb. unit)
1.0
0.8
0.6
0.4
0.2
0.0
400
450
500
550
600
650
700
Wavelength (nm)
10 mA
70 mA

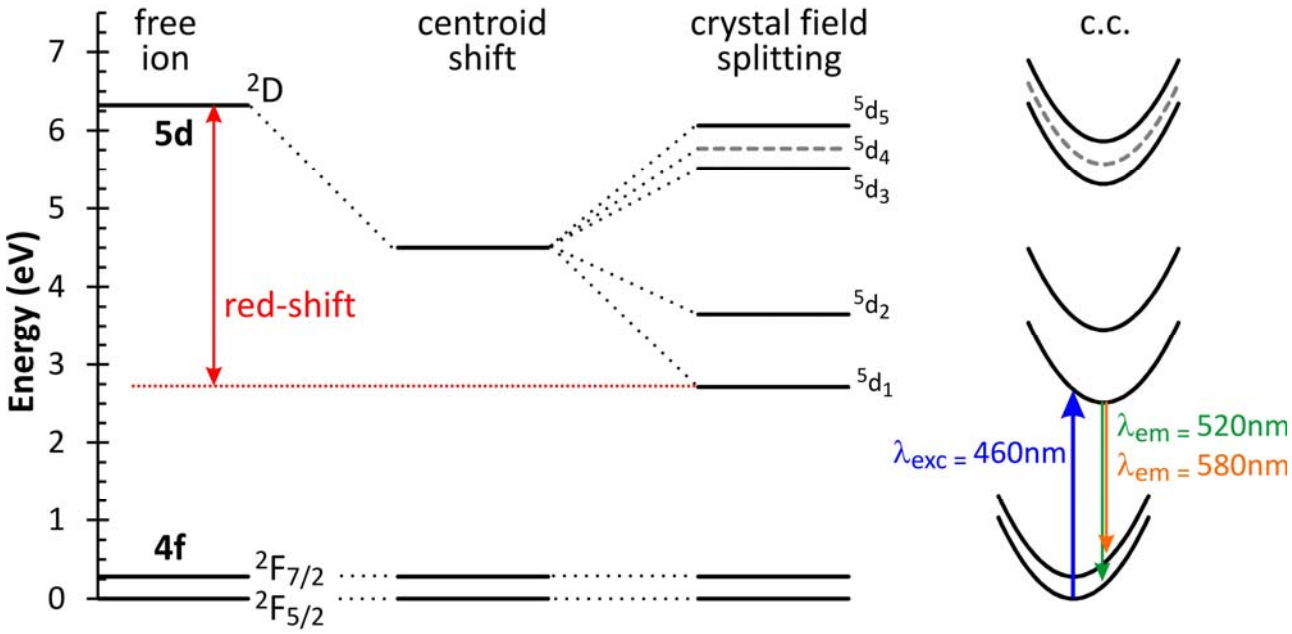
free ion
centroid shift
crystal field splitting
c.c.
Energy (eV)
7
6
5
4
3
2
1
0
5d
4f
2D
2F7/2
2F5/2
red-shift
5d5
5d4
5d3
5d2
5d1
λexc = 460nm
λem = 520nm
λem = 580nm

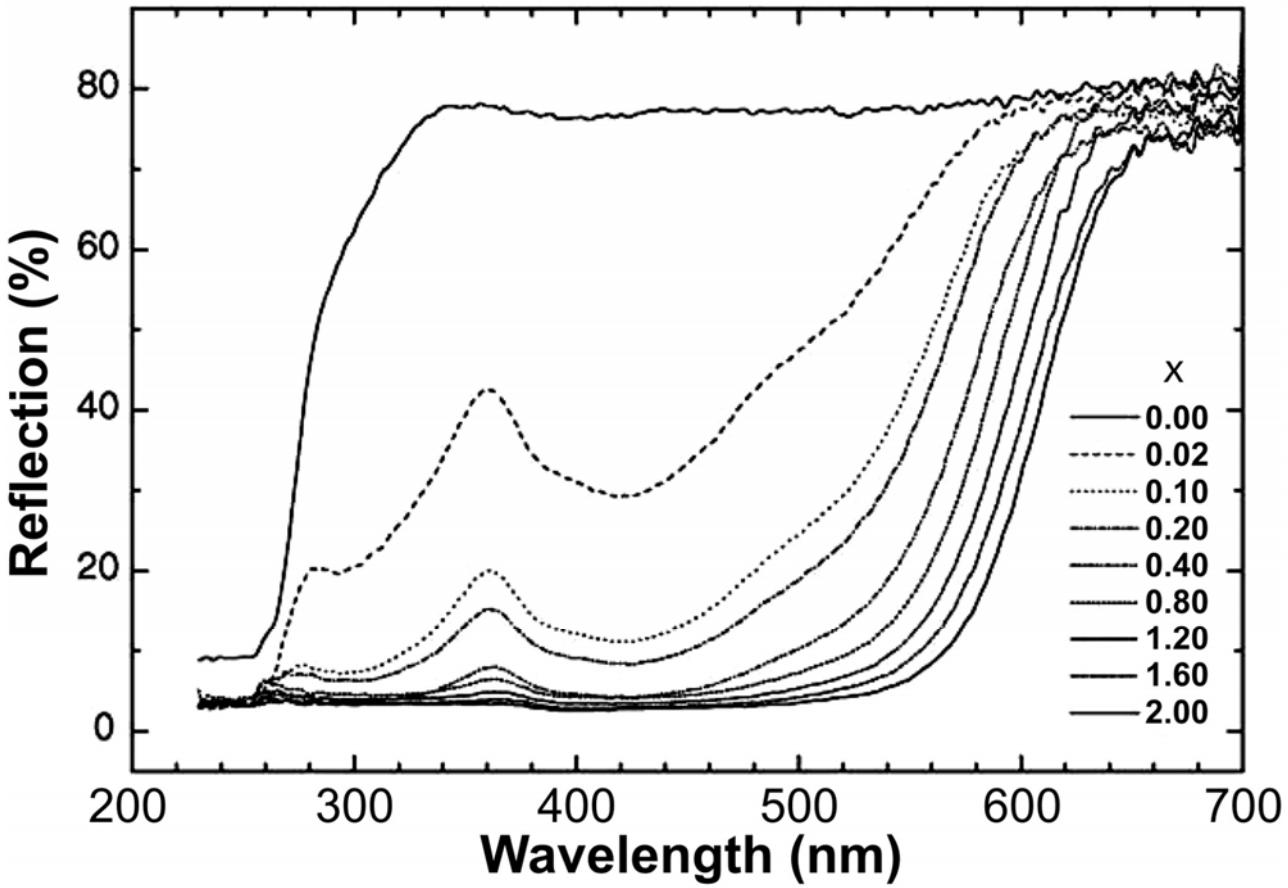
Reflection (%)
0
20
40
60
80
200
300
400
500
600
700
Wavelength (nm)
X
0.00
0.02
0.10
0.20
0.40
0.80
1.20
1.60
2.00

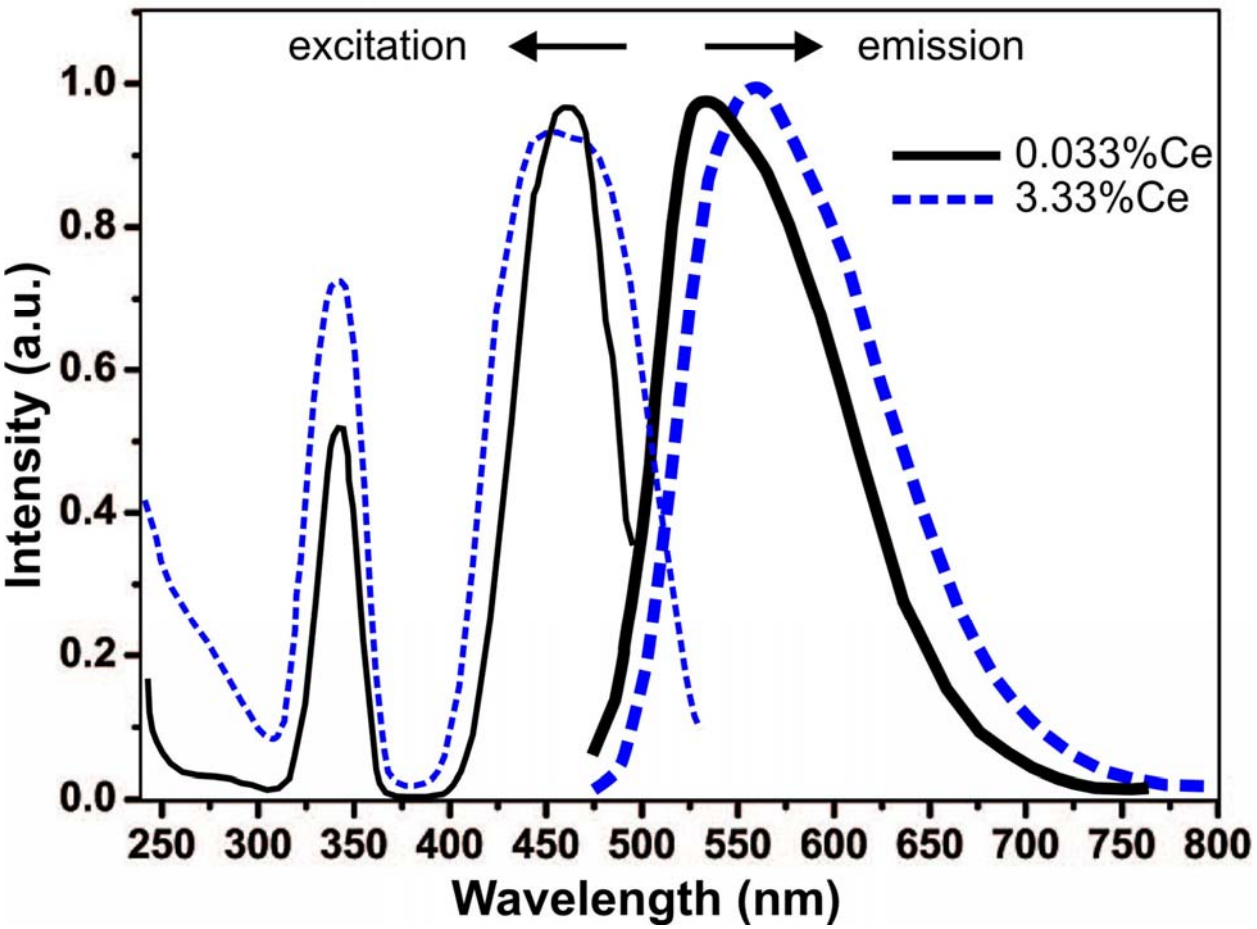
excitation
emission
0.033%Ce
3.33%Ce
Intensity (a.u.)
0.0
0.2
0.4
0.6
0.8
1.0
250
300
350
400
450
500
550
600
650
700
750
800
Wavelength (nm)

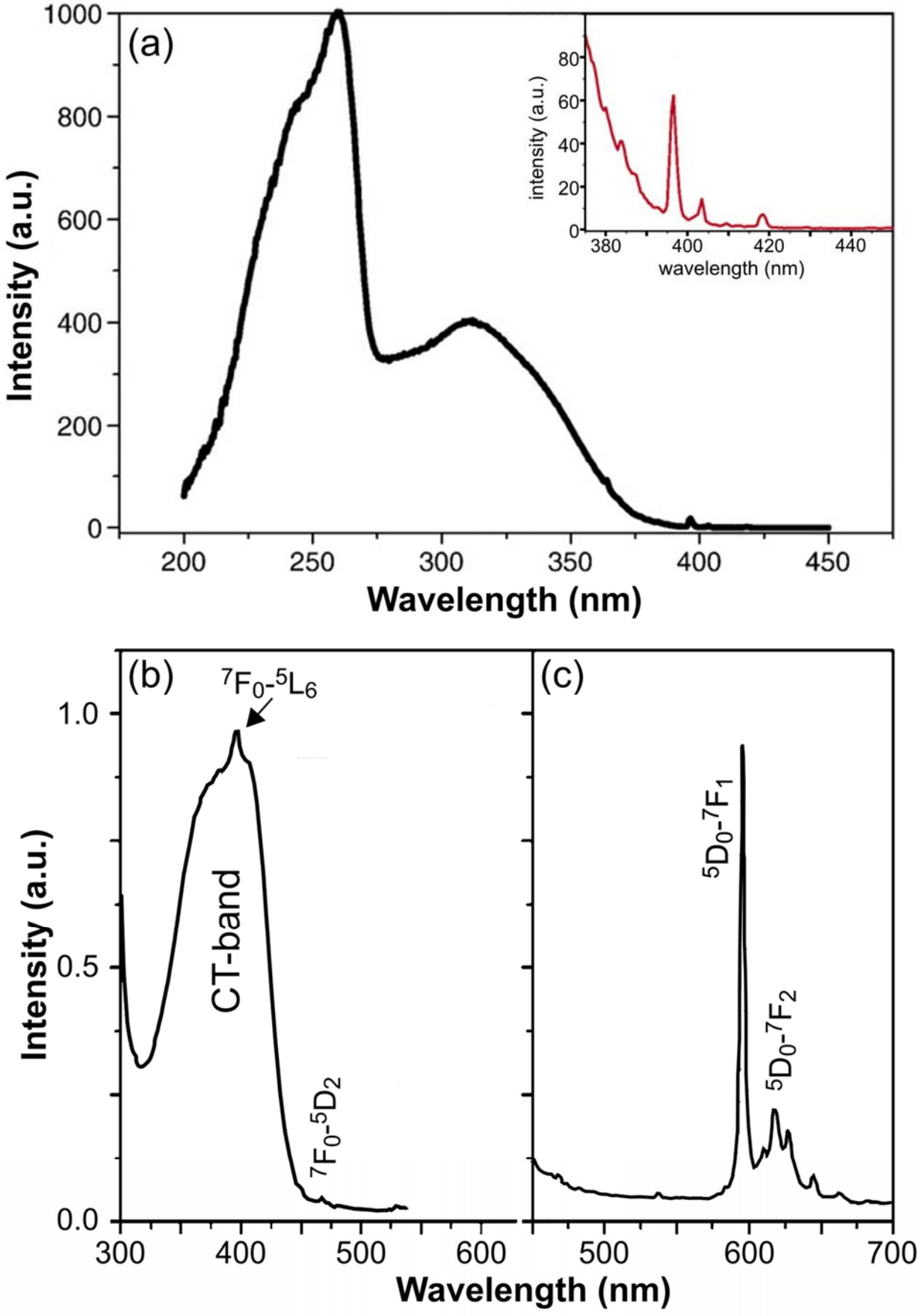
(a)
Intensity (a.u.)
Wavelength (nm)
intensity (a.u.)
wavelength (nm)
(b)
$^7F_0$-$^5L_6$
CT-band
$^7F_0$-$^5D_2$
(c)
$^5D_0$-$^7F_1$
$^5D_0$-$^7F_2$
Intensity (a.u.)
Wavelength (nm)

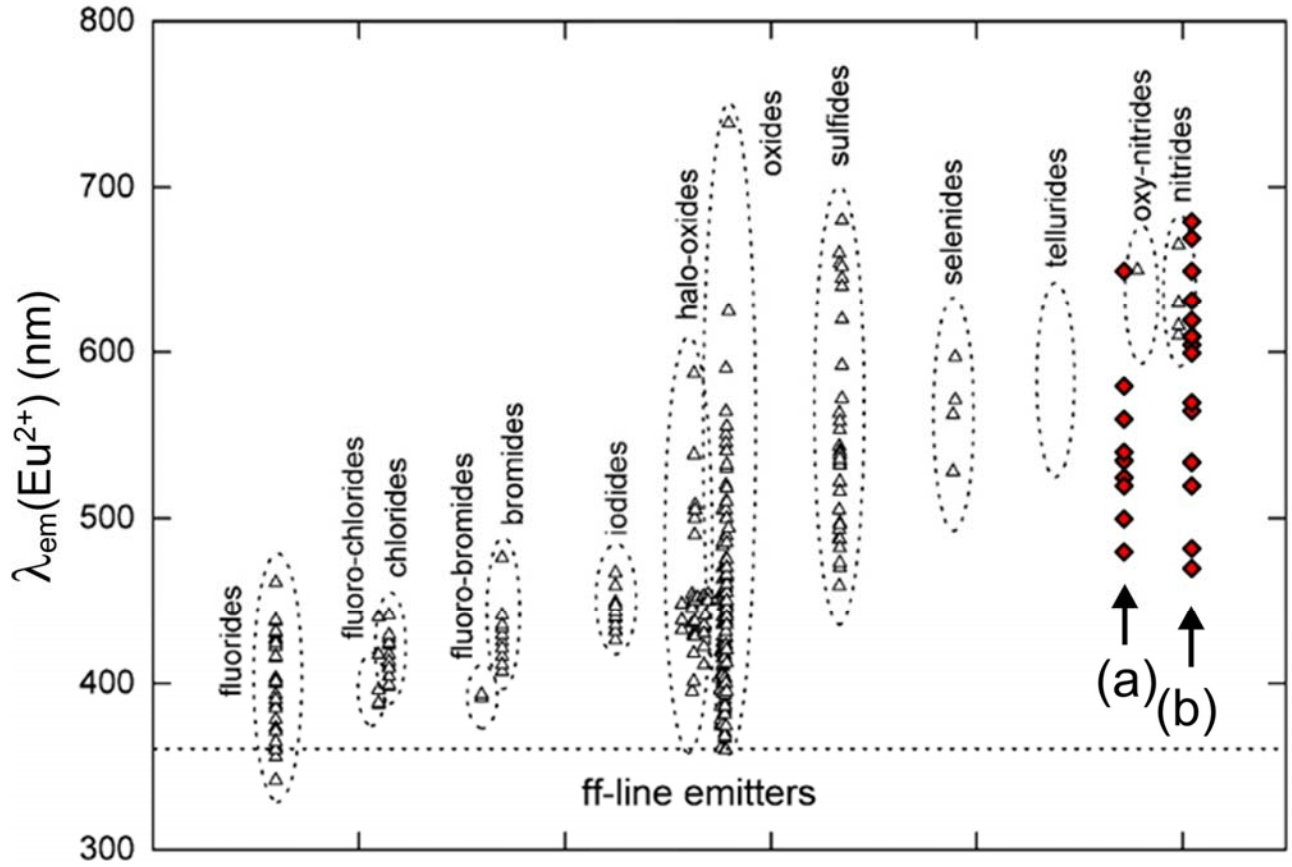
800
700
600
500
400
300
$\lambda_{em}(Eu^{2+})$ (nm)
fluorides
fluoro-chlorides
chlorides
fluoro-bromides
bromides
iodides
halo-oxides
oxides
sulfides
selenides
tellurides
oxy-nitrides
nitrides
(a)
(b)
ff-line emitters

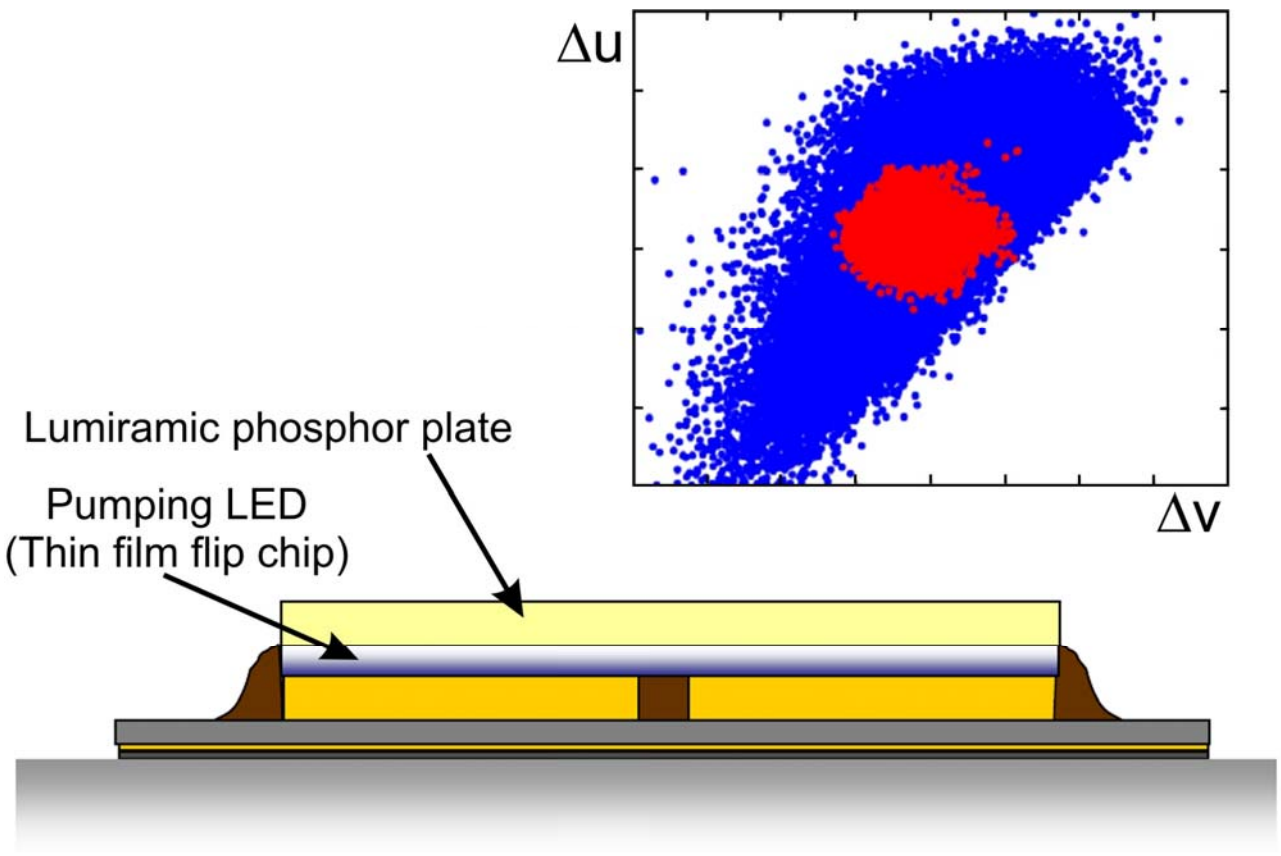
Δu
Δv
Lumiramic phosphor plate
Pumping LED
(Thin film flip chip)

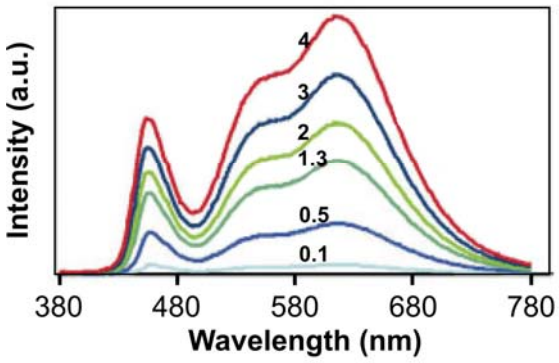
Intensity (a.u.)
4
3
2
1.3
0.5
0.1
380
480
580
680
780
Wavelength (nm)

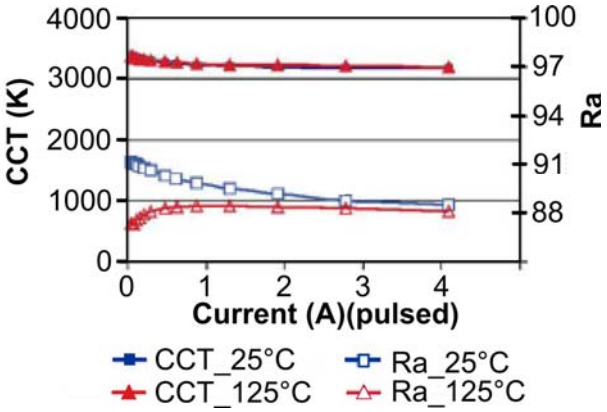
CCT (K)
4000
3000
2000
1000
0
100
97
94
91
88
Ra
0
1
2
3
4
Current (A)(pulsed)
CCT_25°C
Ra_25°C
CCT_125°C
Ra_125°C

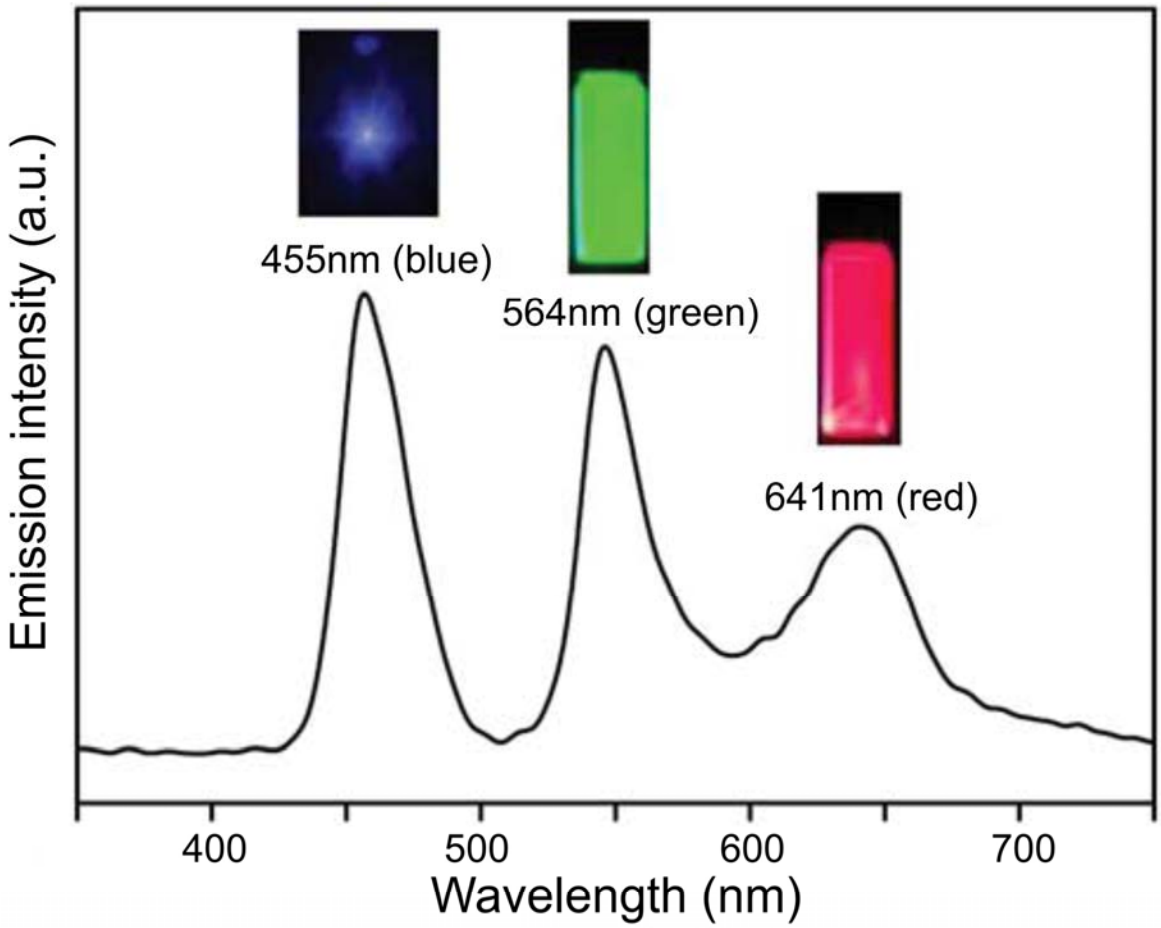
Emission intensity (a.u.)
455nm (blue)
564nm (green)
641nm (red)
400
500
600
700
Wavelength (nm)